UNIMORE
UNIVERSITÀ DEGLI STUDI DI
MODENA E REGGIO EMILIA

UNIVERSITÀ DEGLI STUDI
DI MODENA E REGGIO EMILIA

Dottorato di ricerca in "Ingegneria industriale e del territorio Enzo Ferrari"

Ciclo XXXVIII

Field assisted processing routes for surface finishing and powder reuse in L-PBF

Candidato:	Marco Cardu
Relatore (Tutor):	Prof. Paolo Veronesi
Correlatore (Co-Tutor):	Prof.ssa Elena Colombini
Coordinatore del Corso di Dottorato:	Prof. Alberto Muscio

Sintesi

La tecnologia Laser Powder Bed Fusion (L PBF) consente la fabbricazione di componenti metallici con geometrie complesse e un elevato controllo dimensionale. Tuttavia, la presenza di rugosità superficiale, discontinuità vicine alla superficie, eterogeneità microstrutturali e tensioni residue continua a rappresentare un limite rilevante per applicazioni in cui la resistenza a fatica e la durabilità in esercizio sono requisiti primari. In questo contesto, la tesi sviluppa un quadro integrato per comprendere e governare il ruolo della superficie e dei difetti prossimi alla superficie nella risposta a fatica di componenti in AlSi10Mg prodotti mediante L-PBF, ponendo particolare attenzione a strategie di post-elaborazione capaci di intervenire in modo mirato sulla qualità superficiale e sullo stato del materiale.

L'attività sperimentale è stata condotta su provini realizzati in AlSi10Mg e sottoposti a differenti percorsi di post processing, combinando trattamenti termici e finiture superficiali. In particolare, la distensione è stata adottata come trattamento di base per la riduzione delle tensioni residue, mentre il trattamento T6 (solubilizzazione e invecchiamento artificiale) è stato impiegato per promuovere l'omogeneizzazione microstrutturale e la precipitazione controllata delle fasi di rinforzo. A livello superficiale, sono state confrontate due strategie: una finitura meccanica tramite sabbiatura e una finitura chimica tramite chemical milling in soluzione alcalina, intensificato da irraggiamento a microonde. Quest'ultima è stata implementata come tecnica field assisted, in cui l'interazione elettromagnetica con il mezzo reattivo può indurre condizioni di riscaldamento localizzato e quindi modulare la cinetica di dissoluzione, con l'obiettivo di ottenere una rimozione selettiva e controllata del materiale superficiale.

La caratterizzazione multi scala ha incluso analisi microstrutturali su sezioni, valutazioni di densità e porosità, misure topografiche e di rugosità tridimensionale, oltre a indagini SEM ed EDXS finalizzate a chiarire i siti e i meccanismi di innesco della cricca. Le prove di fatica sono state eseguite in trazione compressione a carico completamente alternato ($R = -1$), fino a 3×10^6 cicli, così da mettere in relazione i risultati di vita e di limite di fatica con i descrittori della superficie e con l'integrità microstrutturale.

I risultati sperimentali evidenziano che la risposta a fatica è governata principalmente dalla qualità della superficie e dalla severità dei difetti prossimi alla superficie, più che

dalle differenze di porosità volumetrica, risultata complessivamente bassa e comparabile tra i batch analizzati. La combinazione invecchiamento più sabbiatura ha mostrato le prestazioni più elevate, con un limite di fatica pari a 115 MPa a 3×10^6 cicli. Al contrario, il chemical milling ha mostrato una maggiore sensibilità alle condizioni microstrutturali e termiche del materiale, con una tendenza ad accentuare discontinuità superficiali e a mettere in evidenza eterogeneità locali, specialmente quando applicato dopo l'invecchiamento. Le osservazioni frattografiche e l'analisi dei siti di innesco indicano che, nei campioni sottoposti a chemical milling, la morfologia delle irregolarità near surface e la loro distribuzione favoriscono stress concentration più elevati e una maggiore dispersione dei risultati di vita, coerentemente con l'ordine osservato nelle curve S-N.

Nel complesso, la tesi dimostra che una finitura meccanica controllata può risultare più efficace di un trattamento chimico nel migliorare la resistenza a fatica dell'AlSi10Mg L-PBF, soprattutto quando integrata con un trattamento termico che stabilizza e omogeneizza la microstruttura. Al tempo stesso, l'analisi della finitura chimica assistita da microonde contribuisce a chiarire opportunità e criticità delle tecniche field assisted applicate al post processing, evidenziando come la non uniformità locale dell'azione chimica possa trasformarsi in un fattore penalizzante se non accompagnata da un adeguato controllo dei parametri di processo e della risposta microstrutturale.

Infine, i risultati sperimentali vengono messi in relazione con una prospettiva più ampia di sostenibilità e circolarità dei processi di additive manufacturing. In tale ottica, la discussione si estende al ruolo di tecniche field assisted anche nella gestione delle polveri esauste, introducendo lo Spark Plasma Sintering come possibile via di valorizzazione e upcycling di polveri degradate da L-PBF. Questa connessione fornisce una chiave interpretativa unitaria, in cui il controllo della superficie e la gestione del ciclo di vita della polvere concorrono, con logiche diverse ma complementari, a migliorare affidabilità, prestazioni e sostenibilità dell'intero ecosistema produttivo.

Synthesis

Laser Powder Bed Fusion (L-PBF) enables the fabrication of metallic components with complex geometries and high dimensional accuracy. Nevertheless, surface roughness, near-surface discontinuities, microstructural heterogeneities, and residual stresses remain significant barriers to fatigue-critical applications, where durability and reliability under cyclic loading are essential. Within this framework, the present thesis develops an integrated understanding of how surface integrity and near-surface defect severity govern the fatigue response of AlSi10Mg components produced by L-PBF, with a specific focus on post-processing strategies that can tailor the surface state and material condition.

The experimental programme was carried out on AlSi10Mg specimens manufactured by L-PBF and subjected to different post-processing routes combining heat treatments and surface finishing operations. Stress relieving was adopted as a baseline step to mitigate process-induced residual stresses. At the same time, a T6 treatment (solution heat treatment followed by artificial ageing) was applied to promote microstructural homogenisation and controlled precipitation of strengthening phases. At the surface level, two alternative approaches were compared: mechanical finishing via sandblasting and chemical finishing via alkaline chemical milling intensified by microwave irradiation. The latter was implemented as a field-assisted technique, in which the interaction between the electromagnetic field and the reactive medium can promote localised heating and thereby modify dissolution kinetics to achieve selective and controlled material removal.

A multi-scale characterisation framework was adopted, including microstructural analyses of cross sections, density and porosity assessment, three-dimensional surface topography and roughness measurements, and SEM and EDXS investigations to identify crack initiation sites and mechanisms. Axial fatigue tests were performed under fully reversed loading ($R = -1$) up to 3×10^6 cycles, allowing fatigue life and endurance limits to be directly linked to surface descriptors and microstructural integrity.

The results demonstrate that fatigue performance is primarily controlled by surface quality and near-surface defect severity, rather than by differences in bulk porosity, which were overall low and comparable across the analysed batches. The combination of ageing and sandblasting achieved the best fatigue response, with an endurance limit of

115 MPa at 3×10^6 cycles. Conversely, chemical milling showed greater sensitivity to the alloy's microstructural and thermal state. It tended to accentuate near-surface discontinuities and reveal local heterogeneities, particularly when applied after ageing. Fractographic observations and crack initiation analyses indicate that, under chemically milled conditions, the morphology and distribution of near-surface irregularities lead to higher stress concentrations and a broader scatter in fatigue lives, consistent with the observed ordering of the S-N response.

Overall, the thesis shows that controlled mechanical surface finishing can be more effective than chemical treatments in enhancing fatigue resistance of L-PBF AlSi10Mg, especially when combined with heat treatments that stabilise and homogenise the microstructure. At the same time, the investigation of microwave-assisted chemical milling clarifies both the opportunities and limitations of field-assisted post-processing routes, highlighting that local non-uniformity in chemical action may become detrimental if not supported by adequate process control and careful consideration of microstructural response.

Finally, the experimental findings are discussed within a broader sustainability and circularity perspective. In this respect, the work expands the field-assisted concept beyond surface finishing. It addresses the lifecycle of L-PBF powders, introducing Spark Plasma Sintering as a potential route for the upcycling of exhausted powders. This connection provides a coherent, overarching narrative in which surface integrity control and powder lifecycle management jointly contribute, through complementary mechanisms, to improving the performance, reliability, and sustainability of additive manufacturing for industrial deployment.

Summary

Sintesi I

Synthesis III

Motivation and Research Objectives 1

Industrial and Scientific Context 2

Chapter 1 – State of the Art on Additive Manufacturing 4

1.1 General Introduction and Definitions 4

1.2 AM Technologies for Metals and Polymers 5

1.3 Materials for AM 11

1.4 Post-processing and Treatments 12

1.5 Modelling and Optimisation Strategies 14

1.6 Sustainability and Industrial Perspectives 16

1.7 Research Gaps and Connection to This Work 18

Chapter 2 – Materials and Methods 21

2.1 Sample preparation 21

2.2 Microwave-Assisted Chemical Milling: enhanced localised etching 26

2.3 Microstructure, Porosity, and Surface Characterisation 28

2.4 Mechanical Characterisation 30

Chapter 3 – Results 32

3.1 Microstructure Characterisation 32

3.2 Cross-section microstructure and surface features 36

3.3 Surface Finishing 38

3.4 Mechanical Tests 42

3.5 Fatigue Tests 44

Chapter 4 – Field assisted powder upcycling: Spark Plasma Sintering (SPS) 52

4.1 Introduction to SPS technology 52

4.2 Two seemingly distant processes, a common underlying issue 54

4.3 Exhausted Powder: a constraint and an opportunity 55

4.4 The role of Spark Plasma Sintering in L-PBF powder upcycling 56

4.5 Convergences and divergences between L-PBF and SPS 58

Chapter 5 – General Discussion 60

5.1 Summary of results 60

5.2 Future research directions 62

5.3 Scientific and industrial contribution 63

Conclusion 64

References ..... A

Acknowledgments .....

Introduction

Motivation and Research Objectives

Additive Manufacturing (AM), and in particular Laser Powder Bed Fusion (L-PBF), has profoundly transformed the design and manufacturing of metallic components by enabling unprecedented geometrical freedom, high material efficiency and the production of functionally optimised parts [1]. The increasing technological maturity of metal AM has led to its progressive adoption in high-value industrial sectors, where design complexity and performance requirements are critical [2]. Among aluminium alloys, AlSi10Mg has emerged as one of the most widely adopted materials for L-PBF due to its favourable strength-to-weight ratio, good processability and suitability for lightweight, high-performance applications [3]. Nevertheless, despite the maturity reached by L-PBF technologies, the widespread industrial deployment of AlSi10Mg components in fatigue-critical applications remains limited.

A key limiting factor is not the alloy's intrinsic static strength, but rather the combined effects of surface roughness, near-surface defects, microstructural heterogeneities, and residual stresses introduced during the layer-by-layer manufacturing process. Rapid solidification and repeated thermal cycling, typical of L-PBF, promote the formation of fine cellular microstructures, element segregation, and process-induced defects, which can act as preferential sites for fatigue crack initiation [4]. As a consequence, fatigue behaviour is often governed by surface and near-surface features rather than by bulk material properties, making post-processing strategies a decisive element in determining functional performance and reliability [5].

Within this framework, surface integrity emerges as a central design and process variable. Conventional post-processing routes, including heat treatments and mechanical surface finishing, are widely applied to mitigate residual stresses and reduce surface irregularities. However, these approaches frequently involve trade-offs between effectiveness, material removal, process complexity and industrial scalability. In recent years, increasing attention has been devoted to field-assisted techniques, in which external physical fields are used to intensify or modulate material transformations. Such approaches offer the potential to tailor surface and near-surface conditions locally, opening new perspectives for controlled surface finishing and the optimisation of fatigue-critical components [5].

In parallel, sustainability considerations are becoming increasingly central to the evolution of Additive Manufacturing. Powder degradation during repeated L-PBF cycles is a critical issue from both economic and environmental perspectives. Extending powder lifecycle and developing viable upcycling routes for exhausted powders requires an integrated view that connects surface processing, material integrity and powder reuse strategies. In this respect, techniques such as Spark Plasma Sintering, which also belong to the broader class of field-assisted processes, offer a potential pathway for valorising degraded powders while preserving material performance.

Against this background, fatigue behaviour is not only a critical performance requirement but also a sensitive and comprehensive metric for assessing the effectiveness of surface and near-surface modification strategies. Fatigue testing establishes a direct correlation between microstructural characteristics, surface conditions, and service-related performance, making it a valuable method for assessing both traditional and field-assisted post-processing approaches.

Industrial and Scientific Context

The food and beverage sector is a dynamic and continuously evolving industry, fundamental to human health and global well-being. This sector faces significant challenges, including the scarcity of natural resources, environmental pressures, and an increasing demand for high-quality, natural foods without chemical preservatives. These factors highlight the industry's need to address evolving consumer expectations while operating in a highly competitive environment. Innovation is thus crucial for food and beverage companies to differentiate themselves and meet these demands.

From a scientific perspective, technological progress has opened new avenues for the food industry. Research is focused on applying various new technologies to ensure food safety, quality, and sustainability. While non-thermal physical technologies for beverage processing, such as hydrostatic pressure, pulsed electric fields, and ultrasound, are gaining prominence for improving product quality and extending shelf life, a parallel and equally transformative wave of innovation is emerging from advanced manufacturing techniques.

The advent of Additive Manufacturing, or also known as 3D printing, is fundamentally reshaping the capabilities within the food and beverage sector, not only in direct food

printing but, also in the fabrication of robust and high-performance machinery components [6, 7]. Initially recognised for its potential in creating customised food items and personalised nutrition [8, 9, 10], AM's impact extends significantly to the manufacturing of process equipment itself. AM technologies offer unparalleled design freedom, enabling the creation of intricate geometries and optimised structures for components that are challenging or impossible to produce with traditional methods [11]. This capability enables for the development of highly specialised parts, such as custom food holders [12] or functional elements within filling machines, which can lead to enhanced operational efficiency, reduced maintenance, and improved equipment longevity.

Materials such as the aluminium alloy AlSi10Mg are becoming increasingly relevant in this context. Its lightweight properties, excellent strength-to-weight ratio, and good processability via Laser Powder Bed Fusion (L-PBF) make it an ideal candidate for components in contact with food or those requiring high mechanical and thermal performance. However, the application of such materials in the food industry necessitates a rigorous understanding of their behaviour under operational conditions, including their corrosion-fatigue performance [13, 14] and adherence to hygienic design principles [15, 16]. AM-produced AlSi10Mg components must meet stringent surface quality requirements, as excessive roughness can impact cleanability and potentially harbour microbial contamination [17, 18]. Therefore, research into post-processing techniques to optimise surface finish and reduce defects is crucial for wider adoption in this sensitive industry.

The application of advanced disciplines, such as artificial intelligence, is transforming various aspects of the food industry, from quality control and supply chain optimisation to safety monitoring and the development of personalised products. AM integrates seamlessly into this vision of Industry 4.0, alongside technologies such as blockchain, big data, and the Internet of Things, by enabling data-driven design, rapid prototyping, and on-demand production [6, 7, 19]. The integration of AM into innovative manufacturing ecosystems helps in optimise processes, enhances overall quality and safety standards, and supports the creation of innovative, durable, and customised equipment solutions. By enabling the production of optimised, lightweight, and durable components (such as those investigated in this thesis for filling machines), AM directly

contributes to the operational efficiency, sustainability goals, and safety standards crucial for the modern food and beverage industry [20, 21].

Chapter 1 – State of the Art on Additive Manufacturing

1.1 General Introduction and Definitions

Additive Manufacturing, commonly known as 3D printing, represents a transformative paradigm in manufacturing, fundamentally altering the conventional approach to product creation. Unlike traditional subtractive or formative manufacturing methods, AM is defined as a "process of joining materials to make parts from 3D model data, usually layer upon layer". This layer-by-layer material deposition, guided by computer-generated digital models, enables the fabrication of complex three-dimensional objects directly from digital files. The process begins with a 3D model, which is then virtually sliced into thin layers. The AM machine subsequently builds the object one slice at a time, with each successive layer being fused or solidified onto the previous one. This principle enables the conversion of digital electronic models into physical parts with high precision and intricate detail.

The origins of additive manufacturing can be traced back to the 1980s, with the invention of stereolithography in 1987 by Charles Hull, marking the first 3D printing technology. Early applications primarily focused on rapid prototyping, enabling quick and cost-effective design iteration. Over the decades, AM technologies have evolved significantly, expanding beyond polymers to encompass a wide array of materials, including metals, ceramics, and composites. Key milestones include the commercialisation of metal printers, such as Laser Engineered Net Shaping, in 1998 and the introduction of binder jetting technology shortly thereafter.

The key benefits of AM are manifold, offering significant advantages over conventional manufacturing processes. Foremost among these is the unparalleled design freedom, enabling the creation of highly complex geometries, internal structures, and topologically optimised components that are difficult or impossible to achieve with traditional methods. This capability facilitates part consolidation, reducing the number of components in an assembly, which can lead to weight reduction and enhanced functional efficiency, particularly in demanding sectors such as aerospace. Furthermore, AM

contributes to sustainability by minimising material waste, as components are built with only the necessary material, and by potentially shortening supply chains through localised, on-demand production. The digital nature of AM processes also allows for rapid product development cycles, customised production, and reduced tooling costs for small-batch manufacturing.

Additive Manufacturing has transcended its initial role as a prototyping tool to become a comprehensive manufacturing solution with diverse applications across numerous industries. These include, but are not limited to, aerospace, automotive, medical, defence, energy, and consumer goods, where it is utilised for functional parts, tooling, and mass customisation [5]. The continuous advancements in AM technologies, materials, and process control are paving the way for its broader adoption in critical applications, driving innovation and efficiency across various sectors.

The terminology surrounding AM can be varied, with terms like "3D printing", "rapid prototyping", "additive fabrication", and "freeform fabrication" often used interchangeably. However, the ISO/ASTM 52900 standard provides a standardised terminology to ensure clarity and consistency within the field [22]. According to ASTM F2792-12A, AM processes are broadly classified into seven categories, including powder bed fusion, material extrusion, and directed energy deposition, among others. These definitions are crucial for understanding the principles and applications discussed in subsequent sections.

1.2 AM Technologies for Metals and Polymers

Additive Manufacturing encompasses a diverse array of technologies, each employing distinct physical principles to construct objects layer by layer. To standardise terminology and ensure consistent communication within the field, the ISO/ASTM 52900 standard classifies AM processes into seven main categories: Binder Jetting, Directed Energy Deposition, Material Extrusion, Material Jetting, Powder Bed Fusion, Sheet Lamination, and Vat Photopolymerization. While all adhere to the fundamental principle of layer-by-layer construction, they differ significantly in the type of raw material they process, the energy source used, and the resulting material properties and applications. The selection of the appropriate AM technology depends on a multitude of

factors, including the desired material, the component's geometric complexity, required dimensional accuracy, surface finish, mechanical properties, and manufacturing costs.

1.2.1 AM Technologies for Metals

For metal additive manufacturing, two categories are particularly prominent: Powder Bed Fusion and Directed Energy Deposition. These technologies enable the fabrication of complex metallic components with tailored properties for demanding applications across various industries.

Laser Powder Bed Fusion

L-PBF processes for metals are among the most widespread and sophisticated methods for fabricating high-performance metallic components, offering exceptional control over microstructure and mechanical properties [23, 24].

L-PBF is one of the most mature and widely adopted metal AM technologies. The process takes place within a sealed build chamber, typically under an inert atmosphere (e.g., argon or nitrogen) to prevent material oxidation, Figure 1. The key steps are as follows:

- **Powder Bed Preparation**: A roller or a recoater blade uniformly spreads a thin layer of fine metallic powder (typically with a particle size distribution of 15-60 µm) across a build plate. The layer thickness can vary between 20 and 100 µm depending on the machine and material.
- **Laser Scanning and Melting**: A high-power laser (commonly fibre or Yb: YAG) selectively scans the cross-section of the part to be built, based on pre-processed 3D CAD data. The laser energy is absorbed by the powder, causing it to fully melt and form a molten pool (melt pool). The molten metal rapidly solidifies upon cooling, fusing with the underlying layer. The rapid melting and extremely high cooling rates (up to 10^6 K/s) are characteristic of the L-PBF process and significantly influence the final microstructure [25].
- **Layer-by-Layer Construction**: After a layer solidifies, the build plate lowers by an amount equal to the layer thickness, and a new layer of powder is spread. This process repeats until the component is complete. Unfused powder remains loose and acts as support for overhanging geometries, which is then removed post-build.

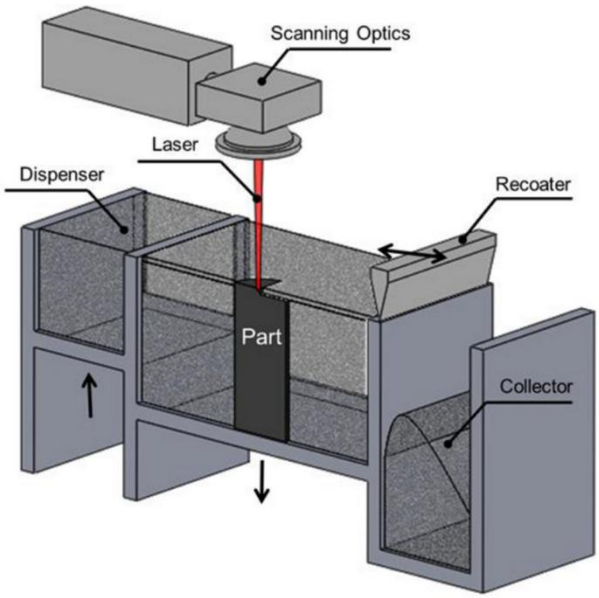

Figure 1 - Schematic representation of the Laser Powder Bed Fusion (L-PBF) additive manufacturing process [26]. The illustration shows the main components of the system: the dispenser, which supplies the metallic powder; the recoater, which spreads a thin and uniform layer over the build platform; the laser and scanning optics, which selectively melt the powder following the CAD-defined pattern; and the collector, which gathers excess material. The build platform lowers incrementally after each layer is fused, enabling the layer-by-layer construction of the part [27].

Table 1 - Main advantages, disadvantages, and typical applications of the Laser Powder Bed Fusion (L-PBF) process. The table summarizes the key characteristics of L-PBF technology, highlighting its potential for achieving high mechanical performance, geometrical complexity, and material versatility, alongside its main limitations such as high production costs, surface roughness, and residual stresses. The information presented provides a comparative overview useful for assessing the suitability of L-PBF in different industrial and research contexts.

Advantages	Disadvantages	Typical Applications
High Density and Excellent Mechanical Properties	LPBF components, especially those made from AlSi10Mg, can achieve near-theoretical densities and exhibit superior mechanical properties, such as enhanced strength, hardness, and dynamic toughness, due to fine microstructures and the absence of binders [23, 24, 28]. The rapid cooling rates result in fine-grained microstructures that significantly enhance properties compared to conventionally manufactured counterparts [25, 29, 30]	High Investment and Operating Costs
Complex Geometries and Topological Optimisation	Allows for the creation of intricate internal structures, lattices, and conformal cooling channels.	Rough Surface Finish
Wide Material Range	Compatible with stainless steels, nickel-based superalloys, titanium alloys, aluminium alloys (like AlSi10Mg), and cobalt-chrome.	Residual Stresses and Distortion
Customisation and On-Demand Production	Ideal for small batches and mass customisation.	Difficulty in Support Structure Removal

Electron Beam Powder Bed Fusion

EB-PBF is another PBF process, similar to L-PBF, that builds metallic parts layer by layer from a powder bed. The primary distinction lies in the energy source: EB-PBF utilises a high-energy electron beam instead of a laser. The process is conducted under a high vacuum, which is obligatory, to allow for electron beam propagation and prevent oxidation of the metallic powder [31].

- **Powder Bed Preheating**: unlike L-PBF, EB-PBF preheats the entire powder bed to elevated temperatures (often between 500-1000 °C, depending on the material) before melting. This preheating significantly reduces thermal gradients and residual stresses [32].
- **Electron Beam Scanning and Melting**: a high-power electron beam selectively scans the cross-section of the part, melting the powder. The electron beam can move much faster than a laser, enabling the melting of multiple areas simultaneously (multi-melt pool strategy) [33].
- **Layer-by-Layer Construction**: similar to L-PBF, the build plate lowers, and a new layer of powder is spread, with the process repeating until the part is complete. The preheated, unfused powder is somewhat sintered, but it is still easily removable.

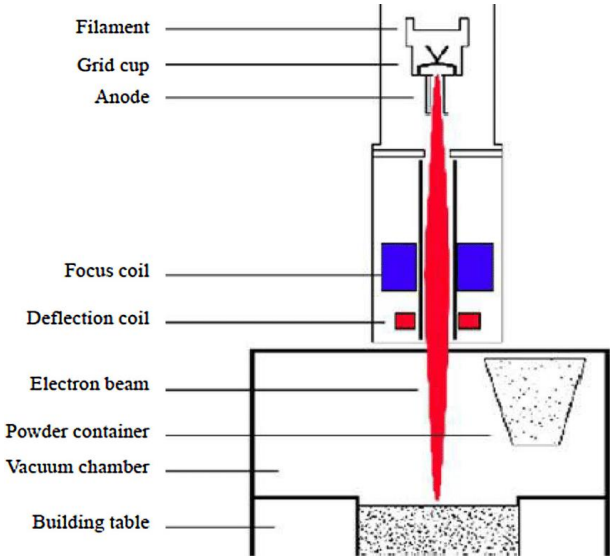

Figure 2 - Schematic diagram of the Electron Beam Powder Bed Fusion (EB-PBF) process [34]. The illustration shows the main components of the EB-PBF system, including the filament, grid cup, and anode, which generate and accelerate the high-energy electron beam. The focus and deflection coils control the beam's precision and scanning path, while the vacuum chamber ensures the required inert environment to prevent powder oxidation. The powder container feeds the build area, and the building table lowers progressively to enable the layer-by-layer construction of the component [35].

Table 2 - Key advantages, disadvantages and typical applications of the EB-PBF process. This table summarises the principal strengths of EB-PBF (such as lower residual stresses, suitability for reactive materials, higher build speed and energy efficiency), alongside its main limitations (including vacuum requirement, inferior surface finish and powder recyclability) and typical industrial deployment areas.

Advantages	Disadvantages	Typical Applications
Lower Residual Stresses	The powder bed preheating drastically reduces thermal gradients, thereby minimising residual stresses and distortion [32].	High Vacuum Requirement
Ideal for Reactive Materials	The vacuum environment is perfect for materials like titanium, which are highly reactive to oxygen at high temperatures [31, 36].	Inferior Surface Finish
Higher Build Speed	The electron beam is faster and can scan multiple areas simultaneously, potentially reducing build times for certain materials and geometries [33].	Lower Resolution
Higher Energy Efficiency	More energy-efficient for melting certain materials.	Less Recyclable Powder

1.2.1.3 Directed Energy Deposition

DED processes are characterised by the simultaneous feeding of material and application of energy to melt it. A key distinction from PBF processes is that in DED, the material (typically in powder or wire form) is fed into a localised melt pool created by an energy source, rather than being pre-placed in a bed.

- **Material Feed**: Material, either as powder blown through nozzles or wire fed from a spool, is directed towards the substrate.
- **Melt Pool Formation**: An energy source (laser, electron beam, or plasma arc) focused on the substrate creates a molten pool.
- **Layer-by-Layer Deposition**: The fed material is melted and deposited into the melt pool, solidifying rapidly to form a new layer. The deposition head moves along the programmed path and typically retracts slightly after each layer to avoid collision with the already solidified material. This allows for direct writing of material onto a substrate.

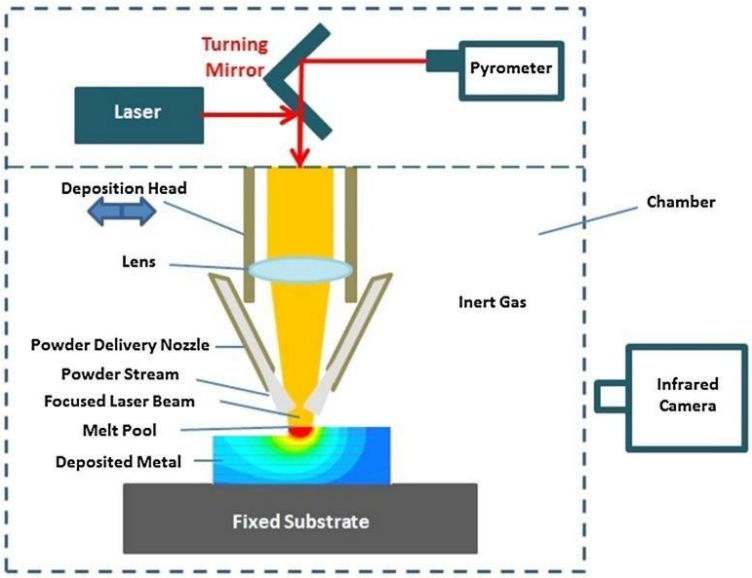

Figure 3 - Schematic representation of the Directed Energy Deposition (DED) process [37]. The image illustrates the main components and operational principle of a laser-based DED system. A high-power laser beam, redirected by a turning mirror and focused through a lens, creates a localised melt pool on the fixed substrate. Metallic powder is fed through coaxial delivery nozzles into the melt pool, where it melts and solidifies rapidly to form the deposited layer. The process takes place within a controlled chamber under an inert gas to prevent oxidation, while pyrometers and infrared cameras enable real-time monitoring of temperature and melt pool dynamics [38].

Table 3 - Key advantages, disadvantages and typical applications of the Directed Energy Deposition (DED) process. The table summarises the principal benefits of DED (such as large-component fabrication, repair, and cladding capabilities, multi-material deposition, and material flexibility), alongside its main limitations (for example, rougher surface finish, lower resolution, and higher material consumption) and its common industrial deployment areas.

Advantages	Disadvantages	Typical Applications
Large Component Fabrication	Ideal for producing large parts that would be impractical with PBF technologies.	Rougher Surface Finish and Lower Precision
Repair and Cladding Capabilities	Ability to repair existing components or add functional coatings onto existing surfaces.	Lower Geometric Complexity
Multi-component/Functionally Graded Materials	Possibility to deposit different materials in the same process to create multi-material structures or functionally graded materials.	Higher Material Consumption
Material Flexibility	Compatible with a wide range of metallic powders and wires.	

1.3 Materials for AM

The rapid evolution of Additive Manufacturing technologies has been paralleled by significant advancements in the range and types of materials that can be processed, dramatically expanding the scope of its applications. Initially dominated by polymers for prototyping purposes, the material landscape of AM now spans a broad spectrum, including advanced metals, ceramics, and various composite formulations, each offering unique properties tailored to specific industrial demands. This material diversity is a cornerstone of AM's disruptive potential, enabling the production of parts with tailored performance characteristics.

Among metallic materials, which are of relevance for high-performance engineering applications, a variety of alloys have been successfully adapted for AM processes. These include stainless steels (e.g., 316L), nickel-based superalloys (e.g., Inconel 718), titanium alloys (e.g., Ti-6Al-4V), and cobalt-chrome alloys, all selected for their excellent mechanical properties at elevated temperatures, corrosion resistance, or biocompatibility. However, the aluminium alloy AlSi10Mg has emerged as one of the most promising and widely investigated materials for AM, particularly when processed via Laser Powder Bed Fusion.

AlSi10Mg is a hypoeutectic aluminium alloy with a nominal composition of 10% silicon and small additions of magnesium. This specific composition imbues the alloy with several highly desirable properties: it is lightweight, possesses an excellent strength-to-weight ratio, and exhibits good weldability. These attributes collectively make AlSi10Mg an ideal candidate for applications demanding high mechanical and thermal performance, particularly in sectors where weight reduction is critical, such as aerospace, automotive, and increasingly, specialised machinery. The near-eutectic composition of AlSi10Mg is especially beneficial for LPBF processes, as it helps to minimise the risk of hot tearing and cracking during the rapid solidification inherent in AM, contributing to its excellent processability [39, 40].

The unique thermal cycles and rapid solidification rates characteristic of AM processes, especially LPBF, profoundly influence the microstructure and, consequently, the properties of AlSi10Mg. Unlike conventionally cast AlSi10Mg, which typically features a coarse microstructure, AM-produced AlSi10Mg exhibits a remarkably fine-grained microstructure. This is primarily due to the high thermal gradients and high-speed

cooling rates (10^3 – 10^8 K/S) experienced during layer-by-layer fabrication. The rapid cooling suppresses the growth of coarse primary silicon phases and instead promotes the formation of a fine, supersaturated aluminium matrix with a network of fine silicon precipitates [41]. This refined microstructure significantly enhances the material's mechanical properties, including its strength and hardness, compared to its conventionally manufactured counterparts.

Furthermore, the high energy density input during L-PBF leads to the formation of distinct melt pools and their subsequent solidification, resulting in a unique cellular or columnar grain structure. The distribution of silicon within this structure, often forming fine eutectic silicon networks along the cellular boundaries, plays a critical role in dictating the material's mechanical response. Controlling these microstructural features through optimised processing parameters is crucial for achieving the desired performance, particularly for attributes such as fatigue strength, which is a central focus of this research. The ability to produce such refined and tailored microstructures through AM makes AlSi10Mg a material of choice for demanding applications, bridging the gap between superior material properties and complex geometric requirements.

1.4 Post-processing and Treatments

While Additive Manufacturing offers unprecedented capabilities for producing complex geometries, the "as-built" condition of AM components often necessitates further processing steps to optimise their mechanical properties, surface finish, and dimensional accuracy for intended applications [22]. These post-processing and treatment procedures are crucial for overcoming the inherent limitations of the AM process, such as residual stresses, surface roughness, and specific microstructural characteristics that may compromise performance [5].

A primary concern in metallic AM is the presence of residual stresses, which arise from the rapid heating and cooling cycles during layer deposition. These stresses can lead to part distortion, cracking, and a reduction in fatigue life [41]. To mitigate this, heat treatments are widely applied. Stress relief annealing is a common initial step, involving heating the component to a sub-solidus temperature, holding it for a period, and then slowly cooling it. This process allows atomic rearrangement to alleviate internal stresses without significantly altering the microstructure. For AlSi10Mg, however, more

sophisticated heat treatments are frequently employed to tailor its mechanical properties. These often include solution treatment followed by ageing (T6 treatment) [41, 42]. Solution treatment involves heating the alloy to a high temperature to dissolve alloying elements, notably silicon, into the aluminium matrix. Rapid quenching then supersaturates the matrix, after which artificial ageing at a lower temperature promotes the controlled precipitation of fine silicon particles. This precipitation hardening mechanism is critical for enhancing the strength, hardness, and often the fatigue life of AlSi10Mg by modifying the silicon morphology and distribution, which significantly differs from the as-built state [41]. Such treatments can also improve ductility by refining the silicon network and reducing internal stresses.

Beyond bulk material properties, the surface quality of AM parts is also a critical factor. Components produced by Powder Bed Fusion, including LPBF, typically exhibit a noticeable surface roughness due to adhered powder particles and the stair-stepping effect of the layer-wise construction [5]. This roughness can act as a stress concentrator, significantly reducing fatigue resistance, and can also impact tribological performance or aesthetic requirements [14]. Consequently, various surface treatments are applied. Mechanical methods such as machining, grinding, polishing, and shot peening are commonly used [5]. Machining can achieve precise dimensional tolerances and remove rough surfaces. At the same time, shot peening introduces compressive residual stresses on the surface, which is highly beneficial for improving fatigue strength by inhibiting crack initiation [14]. Other treatments, such as abrasive flow machining or chemical etching, can further refine the surface finish.

Another practical post-processing step is the removal of support structures. These structures are often necessary during AM to prevent distortion, anchor the part to the build plate, or support overhanging features. Their removal can be labour-intensive and may require specialised tools, ranging from manual breaking or cutting to electrochemical or waterjet techniques, depending on the material and complexity.

For AlSi10Mg, the selection and sequence of post-processing treatments are significant. The interplay between heat treatment parameters and the unique as-built microstructure (fine cellular structures, supersaturated aluminium matrix) dictates the final mechanical performance, including its susceptibility to corrosion-fatigue [14, 41]. Therefore, a comprehensive understanding of how these post-processing steps modify the material's internal structure and surface integrity is essential for producing reliable and high-

performance components, particularly in demanding applications where fatigue resistance is paramount.

1.5 Modelling and Optimisation Strategies

The inherent complexity of Additive Manufacturing processes, stemming from rapid thermal cycles, intricate phase transformations, and dynamic material interactions, necessitates the development and application of advanced modelling and optimisation strategies. These sophisticated approaches are not merely supplementary tools but are crucial for transitioning AM from an empirical art to a predictable, science-driven manufacturing paradigm. The ability to understand and control these complex phenomena is paramount for effectively minimising defects, significantly enhancing material properties, and ultimately ensuring the reliability and consistent performance of AM components in critical applications.

A significant dimension of these strategies involves AM Process Modelling, where computational techniques, such as the Finite Element Method and Computational Fluid Dynamics, are extensively utilised to simulate the physical events occurring during the fabrication process. These models are designed to accurately predict critical outcomes such as the thermal history within the material, the intricate dynamics of the melt pool, the evolution and distribution of residual stresses, and any resulting structural deformations. By precisely simulating how key process parameters (such as laser power, scan speed, layer thickness, and hatch spacing) influence the transient thermal fields and subsequent solidification, researchers can gain invaluable insights into the resulting microstructure and the macroscopic properties of the component [22]. The true power of physics-based modelling lies in its capacity to explain the fundamental physical interactions and the complex material phase changes that occur, offering a deeper mechanistic understanding that is often challenging to acquire solely through experimental observation. This robust predictive capability is vital for substantially reducing the extensive, time-consuming, and costly trial-and-error experimentation traditionally associated with process development, thereby accelerating innovation.

Furthermore, Material Behaviour Modelling is indispensable for accurately forecasting how additively manufactured components will perform under various operational loads and environmental conditions. Given that materials like AlSi10Mg, when processed via AM, often exhibit unique microstructures (characterised by features such as

exceptionally fine cellular structures, specific silicon precipitate distributions, and inherent anisotropies), traditional material models developed for conventionally manufactured counterparts may not always fully capture their distinctive mechanical behaviour. Consequently, specialised constitutive models and simulation frameworks have been developed to account for these AM-specific microstructural characteristics and their direct impact on critical engineering properties, such as tensile strength, ductility, and, most importantly for this research, fatigue life. For the specific investigation, models that establish robust correlations between the chosen processing parameters, the resulting microstructural features (including aspects such as porosity, grain size, and elemental segregation), and the subsequent fatigue performance are particularly relevant. These advanced material models serve as a vital bridge, connecting the initial AM processing conditions with the ultimate in-service performance and durability of the parts, leading to more reliable design and comprehensive validation processes.

The insights and data derived from these sophisticated modelling efforts directly inform and drive Optimisation Strategies. The overarching objective is to identify and implement optimal sets of process parameters that consistently yield components possessing desired attributes, such as maximised mechanical strength, minimised internal porosity, superior surface integrity, or extended fatigue life, all while simultaneously aiming to reduce manufacturing time and associated costs [5]. Optimisation can be systematically achieved through a variety of advanced techniques, including statistical methods such as Design of Experiments, data-driven approaches like surrogate modelling, and metaheuristic algorithms like genetic algorithms or particle swarm optimisation. These methods are frequently integrated with the powerful predictive capabilities of simulation tools. For example, by running numerous simulations with varying parameters, engineers can accurately determine the optimal process conditions, thereby circumventing the need for a large number of physical prototypes and significantly streamlining the experimental phase [22]. This systematic and data-driven approach is instrumental in mitigating common AM defects, such as lack of fusion, keyhole porosity, and excessive residual stresses, which in turn lead to a substantial improvement in the overall quality, consistency, and reliability of additively manufactured parts.

For critical components manufactured from AlSi10Mg, particularly those destined for demanding industrial applications such as the food and beverage sector, where reliability

and hygiene are paramount, these integrated modelling and optimisation strategies are indispensable. They empower researchers and engineers to achieve precise control over microstructure, surface finish, and mechanical properties, necessary to meet stringent performance requirements, including the crucial aspect of long-term fatigue resistance in highly cyclic environments, such as those found in filling machines. Ultimately, these advanced strategies play a pivotal role in facilitating the broader and more confident industrial adoption of AM in sectors where product performance and durability are non-negotiable.

1.6 Sustainability and Industrial Perspectives

The advent of Additive Manufacturing (AM) has significantly reshaped industrial paradigms, not only by enabling unprecedented design freedom and advanced manufacturing capabilities, but also by introducing a complex and often ambivalent sustainability narrative. From a sustainability standpoint, AM offers notable advantages, particularly in material efficiency. Unlike conventional subtractive manufacturing routes, AM constructs components layer by layer, selectively using material only where required, and thereby reducing raw material waste. Several studies report material savings of 35% to 80% compared with traditional manufacturing processes [43]. This intrinsic efficiency is further enhanced by topology optimisation and lightweight design strategies, which lead to the production of lighter components. In weight-sensitive applications, particularly in transportation, these reductions translate into lower fuel consumption and decreased operational emissions during the use phase [44].

Moreover, the digital nature of AM supports on-demand and localised production, potentially shortening supply chains, reducing transportation-related emissions and minimising inventory waste [43, 45]. The possibility of consolidating multiple parts into a single, functionally integrated component also contributes to reduced material usage, simplified assembly operations and improved functional efficiency. Taken together, these aspects position AM as a promising manufacturing paradigm from a resource efficiency perspective.

However, a comprehensive assessment of sustainability in AM must also address its critical limitations. One of the most relevant challenges is the high energy intensity of many AM processes, particularly those based on metal powder bed fusion technologies

[46]. The need for precise control of temperature, atmosphere and laser energy during melting and solidification, combined with the energy demand of auxiliary systems and post-processing operations, can result in a significant energy footprint during the manufacturing phase [47, 48]. While several studies indicate that AM can reduce energy consumption and CO_2 emissions in specific scenarios, especially when optimised designs and reduced product volumes are considered, these benefits are not universal and must be evaluated across the entire product lifecycle [44, 49].

An additional, often underestimated sustainability issue in metal AM concerns the production, reuse, and disposal of metallic powders. The manufacturing of specialised powders, such as AlSi10Mg, is itself energy-intensive, and repeated exposure to thermal cycling, spatter interaction and atmospheric contamination during L-PBF processing progressively degrades powder properties. Changes in particle morphology, size distribution and surface chemistry adversely affect flowability, laser absorptivity, and melt pool stability, increasing defect susceptibility and process variability. Consequently, industrial practice frequently adopts conservative powder refresh strategies, which limit reuse rates and generate significant amounts of exhausted powder. From both environmental and economic perspectives, powder management and recycling represent key sustainability challenges [50, 51, 52].

In parallel, post-processing operations play a decisive role in the sustainability profile of AM components. Heat treatments and surface-finishing steps are often indispensable for achieving the mechanical performance and surface quality required for industrial deployment, particularly in fatigue-critical applications. However, these operations increase energy consumption, processing time, and material removal, thereby increasing the component's overall environmental footprint. In this context, surface integrity should not be regarded solely as a performance requirement, but also as a sustainability lever. Ineffective or poorly controlled surface finishing may expose subsurface defects, increase stress concentration and reduce fatigue life, leading to premature failure, overdesign or frequent replacement. Conversely, optimised post-processing strategies capable of controlling near-surface defect severity can significantly extend component lifetime and improve resource efficiency over the entire service cycle. From an industrial perspective, AM has evolved well beyond its initial role as a rapid prototyping tool and is increasingly adopted for the production of end-use components across multiple sectors. Aerospace, automotive and medical industries have been early adopters, leveraging AM

for functional parts, tooling and mass customisation [53, 54, 55]. The ability to produce complex geometries with reduced lead times and high design flexibility continues to drive the integration of AM into mainstream manufacturing workflows, supported by advances in materials development, process control and design for additive manufacturing [56]. Importantly, AM is also gaining relevance in specialised industrial sectors such as food and beverage processing. While AM is often associated with the direct printing of food products for personalised nutrition or novel culinary applications [7, 9, 57], its impact extends to the fabrication of critical components for machinery. In particular, the production of robust, lightweight and hygienic components for filling machines using alloys such as AlSi10Mg represents a significant and growing application area [12, 58]. The capability to integrate complex internal channels for fluid handling, develop custom-designed parts for specific product lines and reduce operational loads through lightweighting offers substantial benefits in terms of efficiency and sustainability.

Developing fatigue-resistant AlSi10Mg components for such machinery is especially relevant, as reliability and surface quality directly influence maintenance intervals, operational continuity and compliance with stringent hygiene standards. In this context, surface integrity, fatigue behaviour and powder lifecycle management emerge as interconnected aspects rather than independent optimisation problems. Addressing these elements within an integrated framework is essential to fully exploit AM's potential while meeting both industrial performance requirements and sustainability objectives. Field-assisted techniques, applied to surface finishing and to powder upcycling routes such as Spark Plasma Sintering, provide a promising pathway to bridge these dimensions and to support the transition of additive manufacturing towards more sustainable and industrially robust production systems.

1.7 Research Gaps and Connection to This Work

Despite substantial progress in Additive Manufacturing research over the past decade, several critical gaps remain in understanding and optimising metal L-PBF processes, particularly for fatigue-critical applications. While a vast body of literature has addressed process parameters, microstructural evolution, and static mechanical properties of additively manufactured alloys, translating these findings into reliable, durable, and sustainable industrial components remains incomplete. A first significant research gap

concerns the dominant role of surface integrity in governing fatigue behaviour. Numerous studies acknowledge that the fatigue performance of L-PBF components is often controlled by surface roughness and near-surface defects rather than by bulk porosity or intrinsic material strength. However, much of the existing literature treats surface condition either as a secondary variable or as a purely geometric descriptor, without fully integrating microstructural state, defect morphology and post-processing history into a unified interpretative framework. As a result, the mechanisms through which different surface finishing strategies modify crack initiation behaviour and fatigue scatter remain only partially understood. A second gap lies in the fragmented analysis of post-processing strategies. Heat treatments, mechanical surface finishing and chemical treatments are often investigated independently, making it difficult to assess their combined or sequential effects on microstructure, surface integrity and fatigue performance. In particular, chemical surface treatments are often evaluated primarily for roughness reduction. At the same time, their interactions with microstructural heterogeneities, thermal history, and near-surface defect exposure are rarely addressed systematically. This limits the ability to define robust guidelines for selecting and optimising post-processing routes for fatigue-critical components.

A further and emerging gap concerns the role of field-assisted techniques in post-processing and process intensification. While field-assisted approaches, such as microwave-assisted treatments or electrically activated consolidation processes, are increasingly explored in materials processing, their application to the surface finishing of additively manufactured aluminium alloys remains limited. Existing studies often focus on process feasibility or local effects, without linking these techniques to fatigue performance or to the broader concept of surface integrity control. Consequently, the potential advantages and limitations of field-assisted surface treatments in AM are not yet clearly established, particularly with respect to their impact on fatigue life and dispersion of results.

In parallel, sustainability-related research in AM has evolved mainly along a separate trajectory. Powder reuse, degradation, and recycling are typically discussed from a process-stability or cost perspective. At the same time, their implications for mechanical performance and long-term reliability are seldom integrated into fatigue-oriented studies. This separation has led to a disconnect between investigations on powder lifecycle management and those focused on component performance. As a result, the opportunity

to frame powder reuse and upcycling as part of a coherent, sustainable, and fatigue-resistant AM strategy remains largely unexplored.

This thesis is positioned at the intersection of these research gaps. Rather than addressing fatigue behaviour, surface finishing, and sustainability as isolated topics, the work adopts an integrated perspective in which surface integrity serves as the connecting element between post-processing strategies, fatigue performance, and resource efficiency. By systematically comparing mechanical and chemical surface finishing routes, and by introducing microwave-assisted chemical milling as a field-assisted surface treatment, the study aims to clarify how different post-processing strategies modify near-surface defect severity and crack initiation mechanisms in L-PBF AlSi10Mg. Furthermore, fatigue behaviour is used not only as a performance requirement, but also as a diagnostic tool to evaluate the effectiveness and robustness of surface modification strategies. This approach enables a direct link between surface descriptors, microstructural condition and service-relevant performance metrics. Finally, the thesis extends the field-assisted concept beyond surface finishing by addressing powder lifecycle management and introducing Spark Plasma Sintering as a potential upcycling route for exhausted L-PBF powders. In doing so, the work bridges the gap between component-level performance and process-level sustainability, contributing to a more holistic understanding of additive manufacturing as an integrated production ecosystem. Within this framework, the thesis aims to advance the current state of the art by providing experimental evidence and interpretative tools to support the development of fatigue-resistant, surface-optimised, and resource-efficient AlSi10Mg components for industrial applications.

Chapter 2 – Materials and Methods

2.1 Sample preparation

The experimental investigation utilised two distinct specimen batches, designated B1 and B2, which were produced from AlSi10Mg alloy powders, see Figure 4. These powders were sourced from m4p Material Solutions GmbH, based in Ritterhude, Germany. The additive manufacturing process was conducted using a Sisma MySint300 system, employing Laser Powder Bed Fusion technology. Printing occurred within a rigorously controlled argon atmosphere, maintaining a purity level ≥ 99.999% as the shielding gas, with a fan speed of 1.8 m/s. To ensure optimal build conditions and minimise thermal gradients, the build platform was consistently preheated to 200 °C.

Figure 4 - Building plates of AlSi10Mg specimens as manufactured by L-PBF. The two batches (B1 and B2) were produced with different build orientations, as shown in the top views.

The L-PBF process parameters were meticulously selected based on recommendations from both the powder supplier and the Sisma MySint300 manufacturer for AlSi10Mg, aiming for melt-pool stability, high densification, and minimising keyhole porosity. Key parameters included a layer thickness of 60 μm, a border-hatch distance of 200 μm, a hatching distance of 210 μm, a laser spot size of 100 μm, a scanning speed of 1300 mm/s, and a laser power of 420 W. The chosen border-hatch spacing and laser spot size were carefully calibrated to ensure sufficient track overlap, thereby reducing lack-of-fusion defects while maintaining efficient build productivity. A chessboard scanning strategy was implemented to limit residual-stress accumulation further and manage thermal gradients effectively. Both batches, B1 and B2, see Figure 5, were completed under identical process conditions, with key chamber atmosphere and thermal parameters

(oxygen concentration at 0.3%, relative humidity below 50%, and shielding gas temperature of 23±3 °C) continuously monitored to ensure optimal process stability.

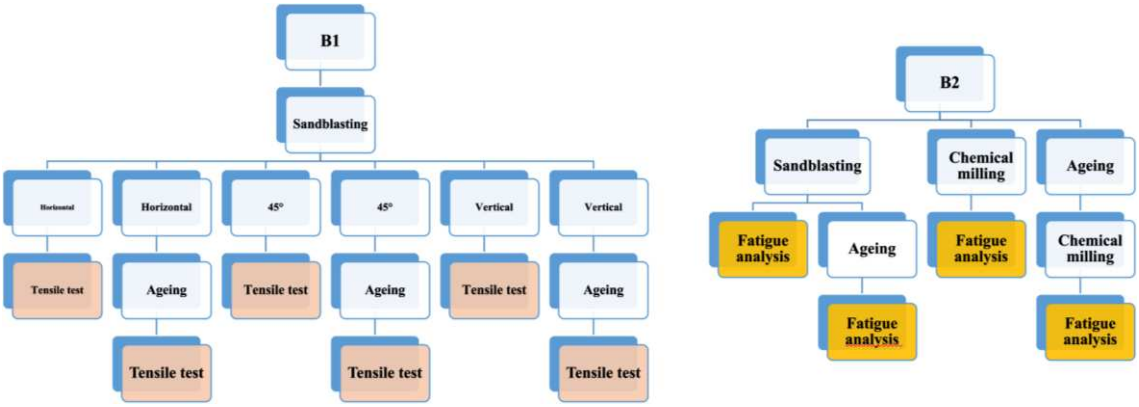

Figure 5 - Schematic view of the specimens produced in two separate batches and respective post-processing and mechanical testing.

Upon completion of the building process and after the two building plates had cooled, excess powder was removed. A representative specimen from each platform (labelled T1 and T2), was then detached for density and porosity assessment through sectioning and image analyses.

Subsequently, both building plates underwent a stress-relief heat treatment designed to mitigate residual stresses inherent from the additive manufacturing process. This treatment was performed in an argon atmosphere for 2 hours at 300 °C, utilising a Nabertherm N60/85 SHA convection furnace. Following this, a T6 heat treatment was applied, consisting of two stages: a solution heat treatment at 505 °C for 4 hours in air, followed by water quenching, and an artificial ageing phase at 200 °C for 4 hours in air. After each thermal step, the specimens were allowed to cool gradually under ambient air.

The specimens from Batch 1 (B1) were allocated explicitly for tensile strength testing. Their geometry was meticulously designed in strict accordance with the ISO 6892-1:2019 standard, which provides comprehensive specifications for the standard dimensions of metallic tensile specimens [37, 59]. Conversely, the specimens from Batch 2 (B2) were prepared for fatigue tests. The geometry of these fatigue specimens was custom-designed to meet the stringent requirements of ISO 12106:2017 [60], a standard that defines the dimensions of cylindrical specimens used in axial fatigue testing of metallic materials. These cylindrical fatigue specimens, see Figure 6, had a precise gauge section measuring 10 mm in diameter and 20 mm in length. The transition between the gripping sections and this gauge section was engineered with a double fillet radius of 30

mm, a design choice aimed at promoting uniform stress distribution and effectively minimising stress concentration in these critical transition zones.

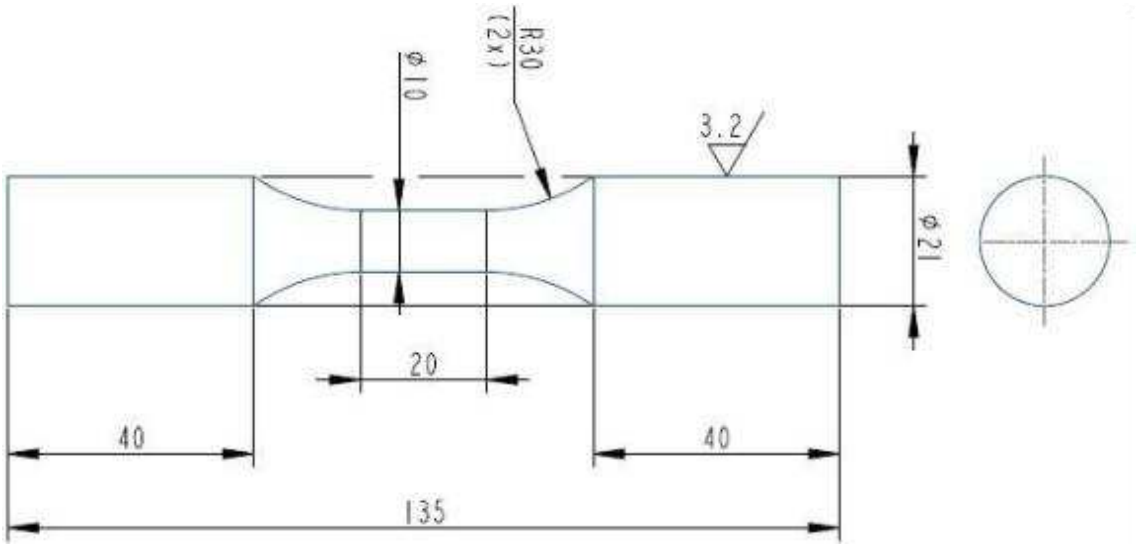

Figure 6 - Geometry of the cylindric fatigue specimen designed according to ISO 12106:2017. The gauge section has a diameter of 10 mm and a length of 20 mm, while the overall specimen length is 135 mm. A double-fillet transition with a 30 mm radius connects the gripping sections to the gauge region.

Following the additive manufacturing process and initial stress-relief heat treatment, a series of post-processing steps was meticulously applied to optimise the surface finish, mechanical properties, and overall integrity of the AlSi10Mg specimens. These treatments included mechanical surface modification via sandblasting, bulk property enhancement through a T6 heat treatment, and targeted surface refinement using microwave-assisted chemical milling. Each process was carefully controlled to ensure consistent and reproducible results, providing a comprehensive understanding of their individual and combined effects on the material.

Sandblasting

After the initial stress-relief heat treatment, a subset of the specimens underwent manual sandblasting. Specifically, nine tensile-test specimens from Batch B1 (out of 18 total) and 40 fatigue-test specimens from Batch B2 were subjected to this mechanical surface treatment. The primary objectives of sandblasting were to improve the surface finish by reducing asperities and to effectively remove any loosely adhered powder particles that remained from the L-PBF process.

The sandblasting operation was performed using corundum (α-Al2O3) as the abrasive medium, selected for its hardness and effectiveness in mechanical surface modification. The abrasive had a grain size of 20-220 µm, delivered at a consistent pressure of 6 bar.

To ensure uniform treatment, the exposure time for each specimen ranged from 60 to 90 seconds. A nozzle-to-surface distance of 15-20 cm was maintained, with the abrasive stream applied at approximately normal incidence to the specimen surface. The process was conducted using a *Lampoblast LC/s system* under controlled laboratory conditions.

Solution Heat Treatment and Artificial Ageing (T6)

An ageing treatment, specifically the T6 thermal treatment, was applied to a subset of the specimens. This is a standard heat-treatment process widely employed to improve the mechanical properties of aluminium alloys, primarily by enhancing their strength and hardness through precipitation hardening. The T6 thermal treatment comprises two distinct stages:

- **Solution Heat Treatment**: Specimens were held at 505 °C for 4 hours in air. The purpose of this stage is to dissolve the alloying elements, notably silicon and magnesium, into the aluminium matrix, forming a supersaturated solid solution. Following this high-temperature soak, the specimens were rapidly quenched in water and subsequently dried. Rapid quenching is critical for retaining alloying elements in solution and preventing premature precipitation.
- **Artificial Ageing**: The quenched specimens were then artificially aged by holding them at 200 °C for 4 hours in air. This lower-temperature treatment promotes the controlled precipitation of fine-strengthening phases, particularly in AlSi10Mg alloys, thereby significantly enhancing the material's mechanical properties. After the ageing phase, the specimens were allowed to cool gradually under ambient air conditions.

Each thermal step was followed by controlled cooling to manage microstructural evolution and prevent the reintroduction of undesirable residual stresses.

Chemical Milling

Chemical milling of the printed parts was performed using a 0.1 M NaOH aqueous solution, enhanced by microwave irradiation. This technique aimed to promote surface smoothing and reduce roughness through a controlled, selective dissolution process. The experimental setup for this advanced treatment was precisely engineered to leverage the benefits of microwave heating.

The setup consisted of a borosilicate glass reactor, positioned within the cavity of a microwave applicator. To ensure optimal homogeneity of the alkaline solution during the process, the system was equipped with a motor-driven stirrer. Continuous temperature monitoring was crucial for process control, and this was achieved using a pyrometer (*IKS-T14-09*, Sitel control Srl, Milan, Italy). The microwave generator's output power was dynamically adjusted throughout the process to maintain the solution temperature consistently within the range of 55-60 °C.

Microwave heating was supplied by a solid-state generator (*LEANGEN-2450M-250-E*, LEANFA Srl, Ruvo di Puglia, Italy), which operated at a frequency of 2.45 GHz. This generator offered fine power adjustment capabilities, allowing increments of 1 W. It also provided real-time measurement of reflected power and operated with a narrow bandwidth. These features collectively ensured stable coupling between the generator and the load, enabling precise control over the power delivered to the treatment cavity. Energy transfer from the generator to the cavity occurred via a coaxial cable connected to a WR340 waveguide through a coaxial-to-waveguide transition and a coupling iris, designed for efficient power matching.

The applicator’s control unit was responsible for regulating both the microwave power and the solution temperature. Initial heating of the NaOH solution was conducted at 150 W for 180 seconds to reach the desired operating temperature. After immersing the component in the preheated solution, the output power was set to 100 W, with the average measured reflected power typically ranging from 1 to 6 W, indicating efficient energy absorption by the solution and specimen. The total immersion time for each component was 300 seconds. To maintain consistent chemical activity and prevent solution degradation, each component underwent four repetitions of this process, utilising a fresh NaOH solution for every cycle. This methodical approach ensured reproducible chemical milling conditions and effective surface refinement.

2.2 Microwave-Assisted Chemical Milling: enhanced localised etching

Microwave-assisted chemical milling represents a promising methodology for modulating material removal by leveraging selective dielectric heating within an aqueous NaOH solution [61, 62]. This advanced technique is rooted in the fundamental interaction of microwaves with the medium, generating an internal electric field. The power density, which reflects the resistive heating generated within the solution, is directly proportional to the square of the electric field intensity ($P \propto E^2$) [63, 64]. This principle governs how electromagnetic energy is converted into thermal energy within the material [63].

When a sample is exposed to an electromagnetic field within an applicator, the distribution of the electric field and consequently the heating is often non-uniform [65, 66]. Studies indicate that areas like the upper and lower surfaces of a liquid medium can exhibit higher field intensities, leading to greater heat generation, while lateral surfaces may experience weaker local fields and reduced heating [65, 66]. This inherent non-uniformity can lead to the formation of "hot spots," which are localised regions of significantly higher temperature within heterogeneous systems or at specific locations on the material's surface [65, 67, 68, 69]. Simulations and experimental observations consistently highlight a concentration of the electric field and, subsequently, heat generation, at surface features such as pronounced roughness and edges [70, 71].

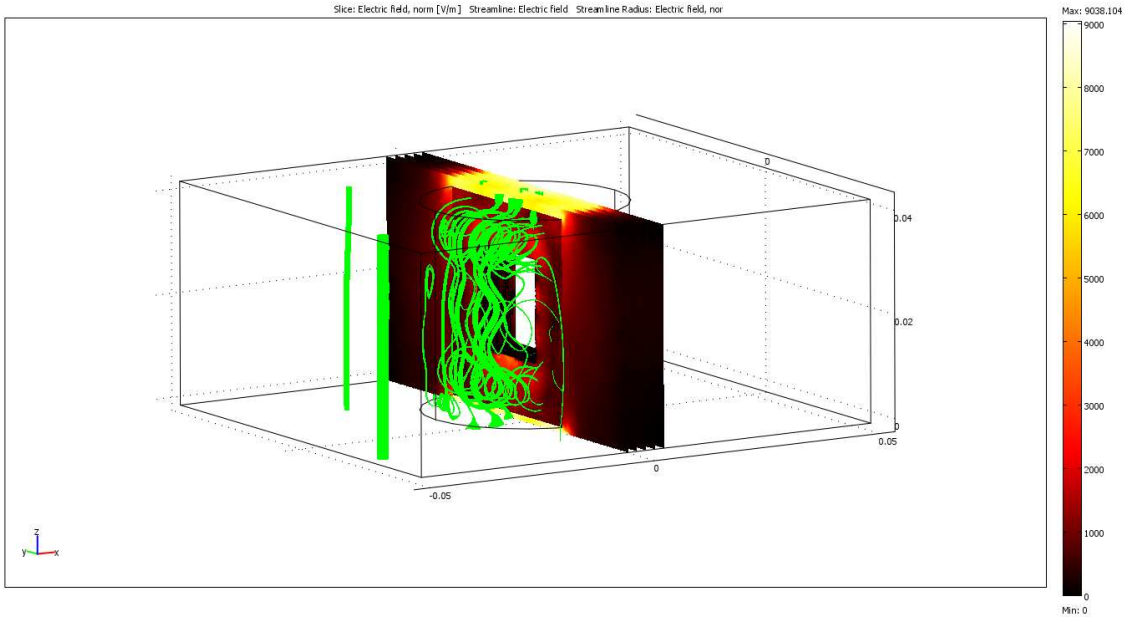

Figure 7 - Three-dimensional simulation of the electric field distribution within the microwave applicator. The colour map represents the electric field magnitude (|E|) along the z-axis, while the green streamlines depict the field lines.

This localised heating mechanism is critical because it selectively increases the chemical reactivity of the solution in these specific areas, thereby promoting preferential dissolution of the material [61, 62]. This selective action explains why regions of the specimens with less intense electric-field exposure may be less affected than areas subjected to greater field exposure. The ability of microwaves to rapidly and selectively induce heating is a key factor in intensifying chemical processes and materials manufacturing [61, 72]. However, the non-uniformity of the electric field and temperature distribution remains an intrinsic challenge in microwave technology, often limiting its application in large-scale processing and requiring careful design and optimisation to achieve desired outcomes and prevent issues like thermal runaway [65, 66, 68, 73, 74, 75]. Precise control over this localised heating, induced by the microwave field, is essential for influencing etching kinetics and the selectivity of the process, opening new possibilities for targeted surface finishing of components with complex geometries [70].

2.3 Microstructure, Porosity, and Surface Characterisation

The as-printed and post-processed components underwent comprehensive characterisation, focusing on both surface morphology and internal structural integrity, including porosity distribution and microstructural features.

Optical microscopy was extensively employed to analyse polished sections, enabling detailed evaluation of internal porosity in representative specimens (T1 and T2) from the two distinct printed batches. This assessment was crucial for verifying the overall print quality and identifying any potential internal defects. To further reveal the intricate microstructural features, polished cross-sections were carefully etched using Keller's reagent for a short duration. This chemical etching process selectively highlighted melt-pool boundaries, the characteristic cellular/dendritic structures commonly observed in L-PBF AlSi10Mg alloys, and any microstructural homogenisation resulting from subsequent heat treatments. Care was taken to ensure the etching process did not alter regions beyond the outermost surface layer. Micrographs of the surfaces of Batch 2 (B2) specimens were specifically acquired to determine surface porosity following various post-processing treatments. Additionally, the two-dimensional surface roughness and the bulk microstructure of these differently treated B2 specimens were thoroughly evaluated from their polished cross-sections. For both surface and bulk porosity determination, image analyses were performed on 10 representative images captured at 200× magnification using ImageJ (version 1.53t, National Institutes of Health, Bethesda, MD, USA).

To accurately assess the density and porosity distributions, specimens from the Batch 1 (B1) were strategically sectioned, see Figure 8. Each sample underwent both longitudinal (L) and transverse (T) sectioning, yielding six distinct sub-sections per sample. These sub-sections corresponded to three different heights along the building direction: Top (T), Middle (M), and Bottom (B). This systematic approach resulted in a classification of the analysed sections as LT, LM, LB (for longitudinal sections) and TT, TM, TB (for transversal sections). (Insert Figure 4: Schematic representation of sample sectioning strategy for determination of bulk porosity distribution using optical microscopy and image analyses (specimen from batch 1)).

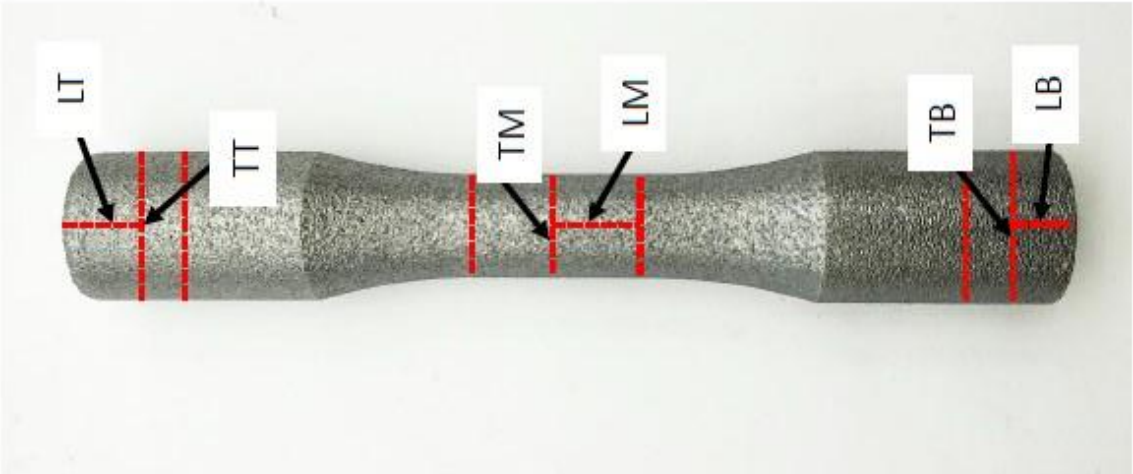

Figure 8 - Schematic representation of sample sectioning strategy for determination of bulk porosity distribution using optical microscopy and image analyses (specimen from batch 1)

Scanning Electron Microscopy played a vital role in assessing the surface morphology and detecting potential contaminants or anomalies. A *JEOL JSM-7610FPlus microscope*, equipped with an Energy-Dispersive X-ray Spectroscopy detector, was utilised for detailed elemental analysis, providing insights into the chemical composition of surface features. Further investigations were conducted at the LAMIS Laboratory of the University of Udine, which is equipped with a *ZEISS Evo 40 SEM* coupled with *Oxford INCA X-Sight and Nordlys EBSD systems*. A critical aspect of the characterisation involved examining the fracture initiation regions of specimens that failed during fatigue tests. This fractographic analysis was essential for understanding the underlying mechanisms of crack initiation and propagation under cyclic loading conditions.

Three-dimensional topographical maps and comprehensive surface roughness parameters were obtained using a noncontact profilometer, operated in structured-light mode. These parameters, including Sa (arithmetic average of the absolute values), Sq (root mean square), Sz (maximum peak-to-valley height), and Sv (maximum valley depth), were calculated in accordance with the ISO 25178 standard [76, 77]. The ISO 25178 standard provides a widely recognised framework for the areal assessment of surface texture, defining various parameters to characterise surface topography [77, 78]. Prior to any analysis, all specimens were meticulously cleaned in ethanol under ultra-sonification to remove any surface debris or contaminants that could interfere with accurate measurements.

2.4 Mechanical Characterisation

The mechanical behaviour of the AlSi10Mg specimens was comprehensively evaluated through tensile and fatigue testing, in accordance with established international standards.

Tensile tests were conducted on specimens printed in various orientations (horizontal, 45°, and vertical) both before and after an ageing treatment. These tests were performed using a servo-hydraulic uniaxial testing machine, *MST 810* (MTS System Corporation, Eden Prairie, MN, USA), equipped with a 100 kN load cell and a high-precision clip-on extensometer with a 25 mm gauge length, equipped with an MTS knife-edge extensometer. The load-displacement data acquired during these tests were subsequently converted into engineering stress-strain curves. From these curves, critical mechanical properties, including yield strength, tensile strength, and elongation percentage, were derived in accordance with the ISO 6892-1:2019 standard [37, 59]. A total of 18 specimens were tested for tensile properties, encompassing three samples for each orientation in both B1 and B2 batches.

Fatigue tests, designed to assess the material's resistance to cyclic loading, were performed on a servo-hydraulic uniaxial testing machine, specifically an MTS 810 model. This system was outfitted with a 100 kN load cell and a hydraulic wedge gripping system, ensuring precise alignment and preventing any slippage of the specimens during the dynamic loading conditions. The machine was also equipped with a high-precision axial extensometer and operated through a closed-loop servohydraulic system. This setup allowed for meticulous maintenance of the prescribed stress ratio and waveform throughout the entire test duration, crucial for obtaining reliable fatigue data. The geometry of the fatigue specimens adhered to the requirements of the ISO 12106:2017 standard [60], which defines the standard dimensions for cylindrical specimens used in axial fatigue testing of metallic materials. Each specimen had a total length of 135 mm, with gripping sections of 21 mm diameter and 40 mm length designed to ensure proper clamping and alignment. The cylindrical gauge section, where stress concentration is intended, featured a diameter of 10 mm and a length of 20 mm.

These fatigue tests were conducted under fully reversed loading conditions (R = -1) at a frequency of 40 Hz, employing a sine waveform. A runout limit of 3×10^6 cycles was established, in accordance with the ISO 12106:2017 standard. The fatigue limit for each

distinct treatment condition was subsequently estimated using the Dixon–Mood method [79, 80]. This staircase approach is particularly well-suited for small sample sets and involves incrementally adjusting the applied stress (in this case ±20 MPa) based on whether a specimen fails or survives within the predetermined cycle limit. This procedure allows for the determination of the median fatigue limit and its statistical uncertainty from the resulting sequence of outcomes.

Each stress level is indexed as i = 0, 1, 2, … relative to a baseline stress S_0. For each level, the number of occurrences of the less frequent event (either failure or survival) is denoted as n_i.

The statistical parameters are then calculated as follows:

Each stress level is indexed as i = 0, 1, 2, … relative to a baseline stress S_0. For each level, the number of occurrences of the less frequent event (either failure or survival) is denoted as n_i.

The statistical parameters are then calculated as follows:

$$A = \sum i\, n_i$$

$$B = \sum i^2\, n_i$$

The mean fatigue limit μ_{DM} is estimated according to:

$$\mu_{DM} = S_0 + \Delta S \left(\frac{A}{N} \pm 0.5 \right)$$

where $N = \sum n_i$, and the sign (±) depends on whether the less frequent event corresponds to a failure (-) or survival (+).

Chapter 3 – Results

The print quality of specimens from batches B1 and B2 was evaluated through porosity analysis of cross-sectional optical microscopy (OM) micrographs. In addition, the tensile-strength characteristics of B1 specimens are presented.

3.1 Microstructure Characterisation

The initial assessment of print quality for specimens derived from both Batch 1 (B1) and Batch 2 (B2) was conducted through a detailed porosity analysis utilising optical microscopy micrographs from cross-sectional views. This characterisation aimed to confirm uniform densification and identify the nature and distribution of any inherent defects. For a comprehensive evaluation, one representative specimen from each printing batch (T1 and T2) underwent meticulous sectioning. Each specimen was sectioned both longitudinally (L) and transversely (T) at three distinct heights along the build direction: Top, Middle, and Bottom. This systematic approach resulted in the analysis of six cross-sections per batch (LT, LM, LB for longitudinal views; TT, TM, TB for transverse views).

The relative density values, presented in Table 4, represent the mean and standard deviation calculated from these six measurements. Across all analysed sections, both builds consistently exhibited high and remarkably uniform densification, see Figure 9. Specifically, relative density values ranged from 99.56% to 99.74% for T1 specimens and from 99.42% to 99.65% for T2 specimens. The detected defect population consisted exclusively of small lack-of-fusion pores, typically measuring less than 20–30 μm and randomly distributed throughout the material. Notably, no gas pores or keyhole porosity were observed, and no systematic variations in defect distribution were detected along the build height or between the two batches.

This indicates stable and repeatable process conditions during additive manufacturing. These findings collectively confirm that the core porosity of both printing batches is extremely low and highly comparable. Given the small size and limited number of these defects, it is anticipated that the bulk porosity will not introduce measurable differences in the subsequent mechanical or fatigue behaviour of the components.

Table 4 - Relative density (%) measured by analysing micrographs collected from various sections of a representative specimen from each printed batch (S1 from batch 1 and S2 from batch 2).

	Top			Middle			Bottom		
	L [%]	T [%]	Mean [%]	L [%]	T [%]	Mean [%]	L [%]	T [%]	Mean [%]
T1	99.69	99.74	99.58±0.14	99.73	99.59	99.66±0.08	99.61	99.56	99.59±0.14
T2	99.61	99.42	99.51±0.14	99.56	99.65	99.61±0.08	99.57	99.55	99.56±0.15

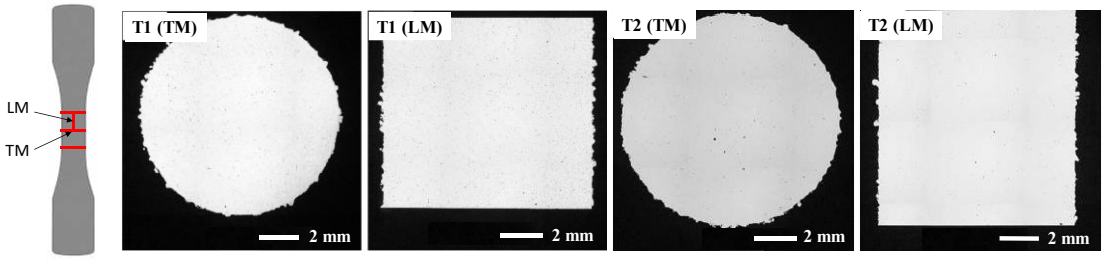

Figure 9 - Optical micrographs of the middle regions of specimens T1 and T2 (representative of printing batch B1 and B2) in both transverse (T) and longitudinal (L) direction.

The consistent densification observed across the top, middle, and bottom regions of the specimens suggests that stable processing conditions were maintained throughout the build. All analysed sections were obtained from two representative specimens, one from each printing batch (T1 from batch B1 and T2 from batch B2), and each specimen was sectioned longitudinally and transversely at three heights, resulting in six analysed regions per specimen. The few observed defects were predominantly minor in size and can be attributed to lack-of-fusion porosity, typically originating from insufficient overlap between adjacent scan tracks or layers. The absence of macroscopic pores or keyhole porosity further confirms the adequate control of process parameters during manufacturing.

Both printing batches (T1 and T2) exhibited comparable densification levels and similar pore populations, with only small lack-of-fusion pores occasionally observed. No systematic variations along the build height or between batches were identified, reinforcing the indication of stable process conditions. These characteristics are typical of well-processed L-PBF AlSi10Mg and are not expected to significantly affect overall mechanical performance. Although small, irregular pores were occasionally observed, their limited occurrence and comparability between batches suggest they are not significant for the subsequent fatigue analysis. Minor differences observed between the two printing batches could be linked to subtle variations in build orientation or chamber atmosphere. Previous studies have indicated that the orientation of the part during laser scanning can influence local solidification dynamics and the resulting defect distribution.

Similarly, the chamber atmosphere plays a critical role in maintaining melt-pool stability and preventing oxide formation. While the oxygen level during printing was controlled to minimise oxidation, slight fluctuations in oxygen content are known to affect melt-pool behaviour and gas entrapment phenomena. Such process instabilities promote the formation of lack-of-fusion or gas-induced pores, potentially leading to small but measurable differences in the relative density of printed batches. This aspect is essential, as the fatigue response of additively manufactured aluminium specimens is predominantly governed by internal defects, such as pores and inclusions, which also primarily determine the fatigue behaviour of cast aluminium alloy components.

Results from image analyses of optical micrographs collected from the external surfaces enabled quantification of surface porosity after the different post-processing treatments. Sandblasted specimens exhibited an average surface porosity of $0.745 \pm 0.624\%$, whereas chemically milled samples showed $0.308 \pm 0.090\%$. While the mean value appears lower for the chemically milled condition, the relatively large standard deviation of the sandblasted samples suggests greater variability rather than a statistically significant difference between the two treatments. This variability can be attributed to the inherent heterogeneity of the manual sandblasting process, which may expose or open pre-existing subsurface pores depending on local impacts and removal depth. Conversely, chemical milling, conducted under more controlled and reproducible experimental conditions, tends to dissolve the outermost layer more uniformly, potentially smoothing the surface and making porosity distribution more homogeneous. However, given the overlap of the error ranges, these results should be interpreted as indicative of different surface morphologies rather than conclusive evidence of varying porosity levels. A similar trend was observed for aged samples, with average surface porosity values of $0.419 \pm 0.296\%$ for sandblasted specimens and $0.259 \pm 0.043\%$ for chemically milled ones (area fraction, %). In both cases, the larger dispersion observed in the sandblasted condition suggests a less homogeneous surface finish, which may influence local stress concentration and fatigue crack initiation. Further analyses, such as pre- and post-treatment mass comparison or 3D surface tomography, are presented in subsequent paragraphs to clarify the relationship between material removal depth and porosity exposure. In addition to surface-connected porosity, the core porosity of the printed material was evaluated on the T1 and T2 specimens extracted from the two build platforms. Image analysis of longitudinal and transverse sections at three heights (top,

middle, and bottom) confirmed a consistently high densification for both builds, with relative densities ranging from 99.42% to 99.74%. Only minor lack-of-fusion defects were detected, typically below the optical resolution limit and randomly distributed, with no systematic variation along the build height. These observations indicate that the bulk defect population is minimal and comparable between the two printing batches. As uniaxial fatigue behaviour in L-PBF AlSi10Mg alloys is primarily governed by internal defects, the very low core porosity measured in both batches suggests that differences in fatigue performance among post-processing routes are dominated by surface condition rather than bulk porosity.

3.2 Cross-section microstructure and surface features

The microstructural characteristics and surface morphology of the specimens, following various post-processing conditions, were thoroughly examined using optical microscopy micrographs collected from cross-sections.

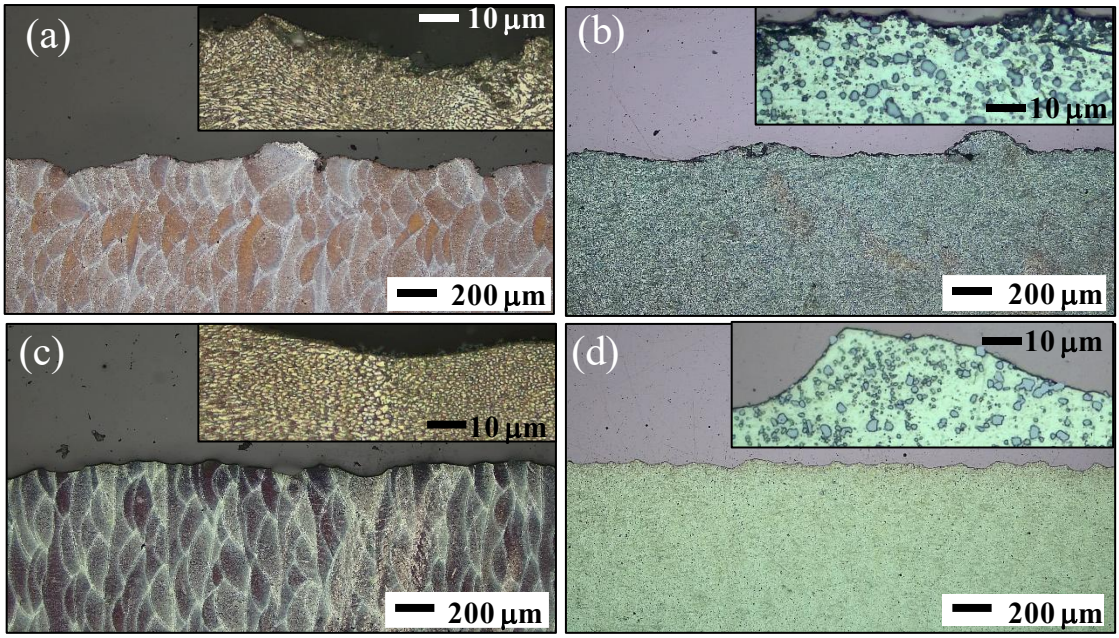

Figure 10 - Cross-section (optical microscope) of a representative specimen for each post-processing conditions: (a) S; (b) S+A; (c) CM; (d) A+CM.

These representative images, complemented by higher-magnification inserts, provided critical insights into both the bulk microstructural features and the alterations to the surface profiles. Two primary distinctions emerged from these observations: first, a clear difference in the bulk microstructure before and after the ageing treatment, irrespective of the surface treatment applied (sandblasting or chemical milling); and second, distinctive surface profiles resulting from sandblasting compared to chemical milling.

Specimens that did not undergo the T6 heat treatment consistently exhibited a typical cellular microstructure. This structure was notably aligned with the solidification direction inherent to the Additive Manufacturing process, with visible scanning traces from the laser path still discernible. In stark contrast, specimens subjected to the ageing treatment displayed a more homogeneous microstructure. In these aged samples, silicon precipitates were uniformly distributed throughout the aluminium matrix, indicating the thermal homogenisation and reduction of dendritic segregation achieved by the T6 heat treatment. This microstructural evolution aligns well with the known effects of T6

treatment on aluminium alloys, which promotes a more refined and consistent internal structure.

Analysing the surface modifications, sandblasted specimens (Figures 10a and 10b) presented an outermost layer that appeared densified and continuous. These samples showed a thin, plastically deformed zone with no evidence of subsurface damage, suggesting that the sandblasting process primarily affected the very surface without creating deeper defects. In the aged and sandblasted condition (Figure 10b), the microstructure displayed a slightly more homogeneous character, with uniformly distributed silicon precipitates, further confirming the stabilising effect of the T6 treatment on the material's internal structure.

Conversely, chemically milled specimens (Figures 10c and 10d) exhibited a thin, irregularly etched surface layer characterised by shallow cavities and a wavy contour, indicative of material removal. The limited depth of this etched layer confirms that the chemical attack, under the investigated conditions, primarily affected only the first few nanometres of the surface. Aged and chemically milled samples (Figure 10d) showed an underlying microstructure that was notably smoother, with silicon precipitates appearing slightly more rounded. This observation is consistent with the microstructural homogenisation promoted by the thermal exposure during the ageing process.

Crucially, across all examined conditions – including sandblasted, aged and sandblasted, chemically milled, and aged and chemically milled – the subsurface microstructure consistently remained dense and free from defects. This significant finding indicates that both sandblasting and chemical milling effectively modify the outer surface characteristics without compromising the bulk integrity of the additively manufactured parts.

3.3 Surface Finishing

A detailed analysis of surface finishing was conducted by acquiring multiple profiles on the gauge section of the fatigue specimens. The average roughness parameters, namely arithmetic mean height (S_a), root mean square height (S_q), maximum peak-to-valley height (S_z), and maximum valley depth (S_v), were calculated for each condition in accordance with ISO 25178-2.

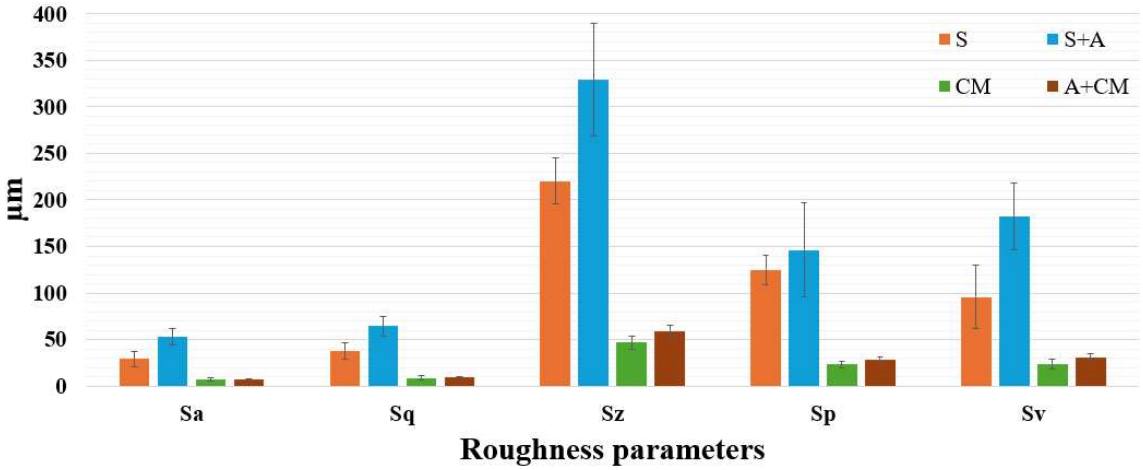

Figure 11 - Surface roughness parameters (Sa, Sq, Sz, and Sv) measured on AlSi10Mg specimens subjected to different post-processing treatments: (a) comparison between chemical milling (CM) and ageing plus chemical milling (A+CM); (b) comparison between sandblasting (S) and sandblasting plus ageing (S+A). Error bars represent the standard deviation from five independent measurements (n=5).

As illustrated in Figure 11, the surface roughness parameters exhibit clear variations depending on the applied surface treatment. Chemical milling and the combined ageing and chemical milling (A+CM) treatments consistently yielded smoother surfaces compared to sandblasting, as evidenced by significantly lower Sa and Sq values. Conversely, sandblasted (S) and sandblasted plus ageing (S+A) specimens displayed higher Sz and Sv values. These higher values are indicative of more profound valleys and more pronounced asperities, which are characteristic features of mechanical abrasion. These observed trends are in strong agreement with the expected surface response to subtractive chemical finishing processes versus mechanical finishing processes.

Further insights into the surface morphology were provided by three-dimensional (3D) profilometry, which highlighted distinct differences across the various post-processing routes.

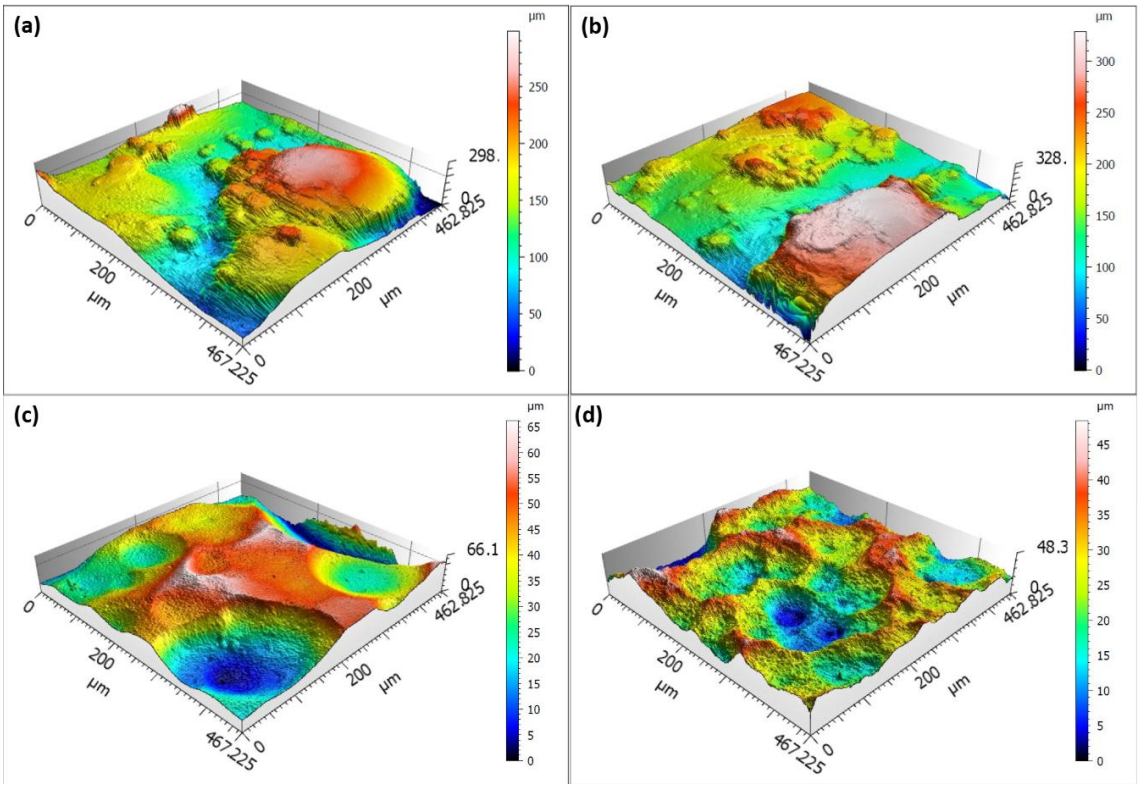

Figure 12 - 3D surface profilometry maps of AlSi10Mg specimens after different post-processing routes: (a) S; (b) S+A; (c) CM; (d) A+CM. Colour bars indicate height (µm) relative to the mean plane.

A striking difference in height distribution was observed among the post-processing routes as depicted in Figure 12. Sandblasted surfaces (Figures 12a–b) exhibited a substantial height range of approximately 300 µm, signifying a rough, heterogeneous, and ridge-dominated topography with large height excursions. The application of ageing (Figure 12b) to sandblasted samples did not remove these macro-features, and the out-of-plane relief remained comparably high. In sharp contrast, chemically milled specimens (Figures 12c–d) showed markedly lower height ranges, typically between 50 and 65 µm. This substantial reduction in amplitude unequivocally confirms the significant smoothing effect achieved by chemical milling. Specifically, the aged and chemical-milled condition (Figure 12d) presented the lowest height range (≈5×10^1 µm) and a visually more homogeneous texture, while chemical milling without prior ageing (Figure 12c) produced intermediate smoothing (≈6×10^{1} µm) with shallow undulations.

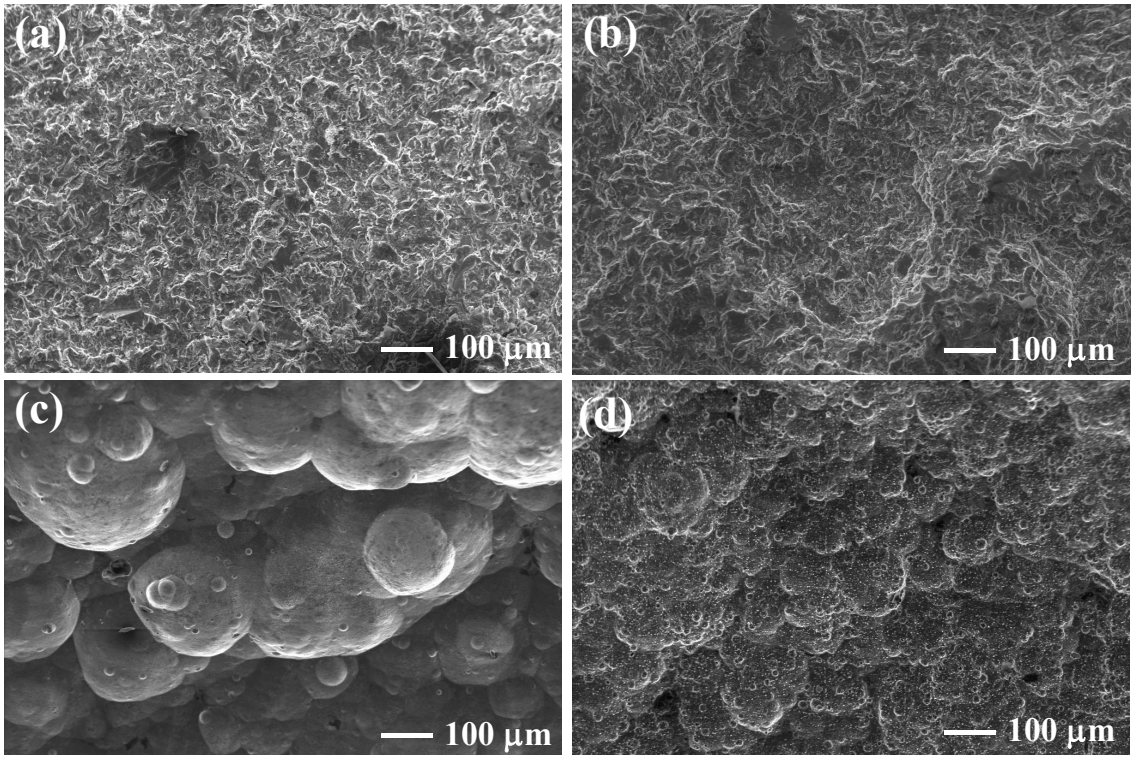

Figure 13 - SE-SEM images of the top surface of specimens subjected to the various post-processing treatments: (a) S; (b) S+A; (c) CM; (d) A+CM.

Figure 13 displays representative Secondary Electron Scanning Electron Microscopy micrographs of the top surfaces of AlSi10Mg specimens subjected to the different post-processing treatments. Sandblasted specimens, both in the stress-relieved (Figure 13a) and aged (Figure 13b) conditions, revealed a homogeneous, finely textured surface. This texture was characterised by overlapping shallow grooves and plastically deformed zones, which are typical indicators of mechanical abrasion. The surface appeared dense and continuous, without any evidence of open porosity or significant cavities. No substantial differences were observed between the stress-relieved and aged states, suggesting that, as anticipated, the T6 treatment primarily influences the bulk microstructure rather than altering the top surface morphology under the investigated conditions.

Conversely, chemically milled specimens (Figure 13c) exhibited a distinctly different surface morphology. This morphology was characterised by rounded protrusions and shallow depressions, resulting from the selective dissolution of the outermost material layer. The resulting topography was more irregular than that of the sandblasted specimens, featuring a fine distribution of these protrusions and shallow depressions across the surface. These morphological changes are consistent with a chemical removal

process targeting near-surface material. Despite these changes, no distinct melt-pool boundaries or segregation bands were visible in the images, confirming that the etching primarily affected the surface layer rather than revealing underlying structural patterns. When ageing preceded chemical milling (Figure 13d), the surface showed a slightly coarser texture and wider etched regions than in the stress-relieved condition. This effect may be attributed to the increased chemical reactivity of precipitate-rich zones developed during the T6 treatment, potentially enhancing local dissolution during etching. Despite these localised differences, the overall morphology remained continuous, with no evidence of deep pits or microcrack formation.

In summary, sandblasting consistently produced a uniform, plastically smoothed surface characterised by mechanical abrasion, whereas chemical milling generated a chemically roughened morphology featuring irregular protrusions. While ageing modified the material's etching response, it did not substantially alter the general topographic features established by the initial surface treatment.

3.4 Mechanical Tests

The mechanical properties of the AlSi10Mg specimens were rigorously assessed through tensile testing, focusing on Batch 1 (B1) specimens printed in various orientations, both before and after an ageing treatment.

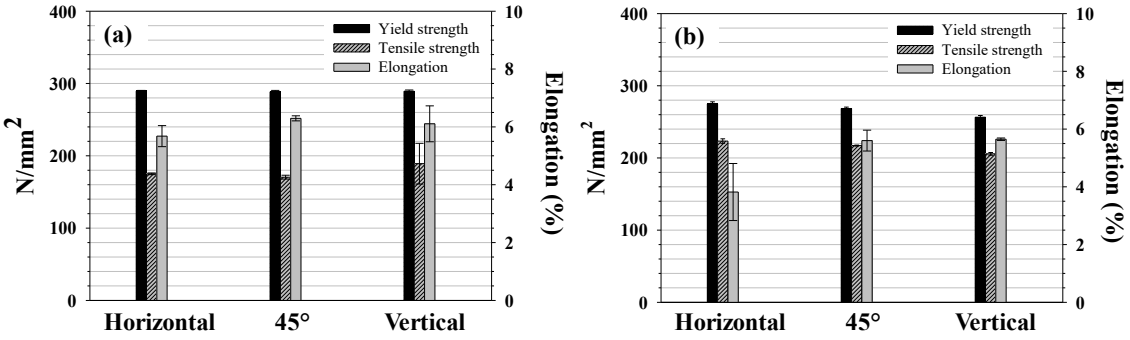

Figure 14 - The yield strength, the tensile strength and elongation for B1 specimens printed in the three different directions before (a) and after (b) ageing. Error bars represent the standard deviation from three independent measurements (n=3).

Figure 14 illustrates the yield strength, tensile strength, and elongation for B1 specimens printed in three different directions: horizontal, 45°, and vertical. Comparing the mechanical response of specimens before (Figure 14a) and after (Figure 14b) T6 ageing, it is observed that the T6 treatment leads to a moderate increase in ultimate tensile strength. Conversely, both the yield strength and elongation exhibit a slight decrease. This overall outcome represents a strength-ductility trade-off, a phenomenon commonly associated with the precipitation of strengthening particles within the aluminium matrix. The T6 heat treatment is known to induce microstructural homogenisation and promote precipitation hardening, which alters the material's mechanical behaviour.

For the non-aged samples (Figure 14a), no statistically significant differences were observed in either yield or tensile strengths across the different printing orientations. The only notable distinction among these samples was a slightly lower elongation recorded for horizontally printed specimens. Following the T6 treatment, the mechanical response was more homogeneous character across the different build orientations (Figure 10b). This homogenisation is an expected consequence of the microstructural changes and precipitation hardening induced by the heat treatment. However, after ageing, both the yield strength and tensile strength were lowest in the vertically oriented samples. In contrast, elongation was lowest for the horizontal orientation, while vertically printed

specimens and those printed at a 45° angle showed no significant difference in elongation.

The subtle variations in mechanical performance observed after ageing can be attributed to the formation of fine-strengthening Mg_2Si precipitates within the aluminium matrix and the progressive homogenisation of the microstructure induced by the T6 treatment [43]. Although the T6 heat treatment is generally expected to enhance the mechanical strength of AlSi10Mg alloys by promoting the precipitation of Mg_2Si phases, the results obtained here indicated a slight decrease in both yield and ultimate tensile strength after ageing. This specific behaviour may be attributed to partial precipitation during the preceding stress-relief treatment, which may already have induced a moderate strengthening effect. Consequently, the subsequent T6 cycle might have reduced solid-solution strengthening due to partial dissolution and reprecipitation, potentially leading to lower strength than in the as-built or stress-relieved condition. While no direct measurements of precipitate size were performed in this study, such a response is consistent with the expected microstructural evolution of AlSi10Mg following solution treatment and ageing. Among the investigated orientations, vertically built specimens exhibited the lowest strength after ageing but maintained comparable elongation to the 45° condition. For this reason, the vertical orientation was selected for subsequent fatigue testing, as it represents a more critical configuration with respect to process-induced anisotropy and defect sensitivity. This choice provides a conservative basis for assessing fatigue performance under cyclic tensile stresses.

3.5 Fatigue Tests

The fatigue behaviour of specimens subjected to various post-processing treatments was meticulously determined, and the results are visually represented in Figure 15, which displays the stress amplitude as a function of the number of cycles to failure (i.e., the S-N curve). The endurance limits for each post-processing condition were estimated using the Dixon–Mood staircase method. To provide full transparency and allow for assessment of the stability and convergence of the staircase series, the complete sequence of applied stress levels, failures, and run-outs for each condition is detailed in Table 5.

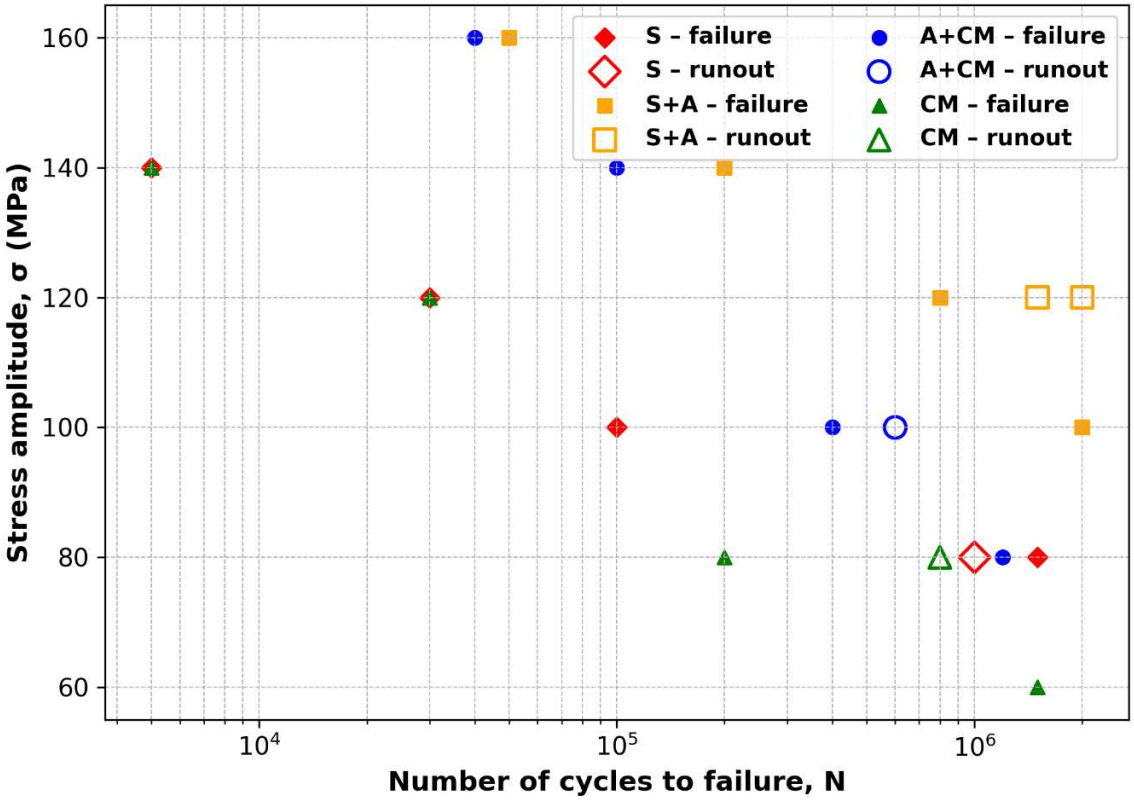

Figure 15 - Stress amplitude as a function of number of cycles to failure (S-N curve). Open symbols represent runouts.

Table 5 - Dixon–Mood staircase data for sandblasted (S), sandblasted and aged (S+A), chemically milled and aged and chemically milled (A+CM) specimens: applied stress amplitude, number of cycles and outcome (F = failure, R = run-out).

Sandblasted (S)						Sandblasted (S) + Aged (A)					
Test	**Specimen**	**σ**	**N**	**Outcome**		**Test**	**Specimen**	**σ**	**N**	**Outcome**	
[-]	**[-]**	**[MPa]**	**[cycles]**	**F**	**R**	**[-]**	**[-]**	**[MPa]**	**[cycles]**	**F**	**R**
1	E41	100	85652	✔		**1**	E61	100	3000000		✖
2	E42	80	3000000		✖	**2**	E62	120	312798	✔	
3	E43	100	129495	✔		**3**	E63	100	3000000		✖
4	E44	80	3000000		✖	**4**	E64	120	2935645	✔	
5	E45	100	167913	✔		**5**	E65	100	3000000		✖
6	E46	80	3000000		✖	**6**	E66	120	589207	✔	
7	E47	100	140864	✔		**7**	E67	100	783362	✔	
8	E48	80	3000000		✖	**8**	E68	80	3000000		✖
9	E49	100	166407	✔		**9**	E69	100	78094	✔	
10	E50	80	3000000		✖	**10**	E70	80	3000000		✖
11	E51	100	174807	✔		**11**	E71	100	3000000		✖
12	E52	80	1854407	✔		**12**	E72	120	1562341	✔	
13	E53	60	3000000		✖	**13**	E73	100	3000000		✖
14	E54	80	3000000		✖	**14**	E74	120	1978509	✔	
15	E55	100	148.868	✔		**15**	E75	100	3000000		✖
16	E56	120	28054	✔		**16**	E76	120	505359	✔	
17	E57	140	5743	✔		**17**	E77	140	186658	✔	
						18	E78	160	50106	✔	

Chemically Milled (CM)						Aged (A) + Chemically Milled (CM)					
Test	**Specimen**	**σ**	**N**	**Outcome**		**Test**	**Specimen**	**σ**	**N**	**Outcome**	
[-]	**[-]**	**[MPa]**	**[cycles]**	**F**	**R**	**[-]**	**[-]**	**[MPa]**	**[cycles]**	**F**	**R**
1	E14	100	157352	✔		**1**	E39	100	495102		✖
2	E13	80	307315	✔		**2**	E22	80	3000000	✔	
3	E7	60	3000000		✖	**3**	E34	100	3000000		✖
4	E8	80	510852	✔		**4**	E40	120	205040	✔	
5	E9	60	3000000		✖	**5**	E36	100	3000000		✖
6	E10	80	528351	✔		**6**	E25	120	417684	✔	
7	E1	60	3000000		✖	**7**	E23	100	3000000		✖
8	E2	80	747751	✔		**8**	E24	120	233159	✔	
9	E3	60	3000000		✖	**9**	E26	100	384721	✔	
10	E4	80	491901	✔		**10**	E27	80	3000000		✖
11	E5	60	3000000		✖	**11**	E21	100	2484801	✔	
12	E6	80	312702	✔		**12**	E37	80	3000000		✖
13	E11	60	3000000		✖	**13**	E38	100	691452	✔	
14	E12	80	408422	✔		**14**	E39	80	1406551	✔	
15	E15	60	1983802	✔		**15**	E30	60	3000000		✖
16	E18	120	28202	✔		**16**	E31	140	103363	✔	
17	E16	140	5932	✔		**17**	E28	160	38283	✔	

Among all tested groups, the sandblasted + aged (S+A) specimens demonstrated the best fatigue performance, with a median fatigue limit of 115 MPa, a 10th percentile of 95 MPa, and a 90th percentile of 135 MPa. Conversely, the lowest fatigue resistance was observed in the aged + chemically milled (A+CM) and chemically milled groups. A+CM specimens showed a median value of 85 MPa (with a 10th-90th percentile range of 75-95 MPa), while CM specimens had a median of 70 MPa (with a 10th-90th percentile range of 60-80 MPa). These values distinctly reflect the varying capabilities of each treatment to influence crack initiation, primarily through modifications to surface morphology and subsurface integrity. The stress-relieved + sandblasted (S) condition displayed a narrow scatter of fatigue lives and a clearer separation between failures and run-outs. This behaviour is consistent with the more uniform surface morphology observed in this group, leading to a more predictable fatigue response compared with the other treatments.

In contrast, the chemically milled specimens exhibited early failures and a narrow range of endurance limits. Most samples failed at pressures below 120 MPa, with only a few reaching the runout threshold, suggesting that chemical milling may expose or exacerbate surface-connected flaws, even without prior ageing. This negatively impacts fatigue life. The most favourable fatigue behaviour was consistently recorded in the sandblasted + aged group. A significant number of these specimens withstood the 3×10^6 cycle threshold at moderate to high stress amplitudes (up to 120 MPa). The synergistic effect of ageing and mechanical surface refinement likely contributed to reducing surface defects and stabilising microstructural features, resulting in a higher endurance limit and reduced fatigue-life scatter. Conversely, specimens that were aged and then chemically milled (A+CM) exhibited a wide dispersion in fatigue life. Failures occurred across a broad stress range, with several instances in the 100–120 MPa interval and only a few runouts observed around 80 MPa. This outcome suggests that chemical milling, when applied after thermal exposure, may amplify surface-connected microstructural discontinuities, thereby reducing fatigue resistance and increasing the variability in failure modes.

The observed trends are consistent with the different ways surface finishing interacts with the material's thermal history. Sandblasting tended to create a uniform, plastically smoothed surface, which, when combined with ageing, provided optimal fatigue resistance. Conversely, chemical milling tended to enhance the local surface relief, producing rounded protrusions and shallow depressions. Particularly after ageing, this

may have accentuated near-surface heterogeneities, leading to earlier crack nucleation and greater variability in fatigue life. Overall, the results indicate a combined influence of the post-processing route and thermal condition on fatigue behaviour: sandblasting is associated with higher endurance limits and reduced scatter, while chemical milling – especially when applied after ageing – correlates with lower fatigue limits and a wider dispersion of lifetimes.

The observed differences in fatigue performance can be further interpreted by explicitly considering the assumptions underlying the present analysis. Given the consistently high relative density measured in all specimens (above 99.4%), bulk porosity effects are assumed to play a secondary role within the investigated stress range, and fatigue behaviour is therefore interpreted as being predominantly surface-driven. This assumption is valid for the specific material state analysed in this work. Still, it may not hold for L-PBF AlSi10Mg components characterised by higher internal defect populations or different build strategies.

Within this framework, the fatigue response emerges as strongly dependent not only on the final surface condition, but also on the sequence of post-processing treatments. The experimental evidence indicates that fatigue behaviour is path-dependent rather than solely state-dependent: identical surface-finishing techniques applied before or after ageing lead to markedly different endurance limits and scatter. In particular, chemical milling performed after ageing appears to interact unfavourably with the thermally stabilised microstructure, amplifying near-surface heterogeneities and increasing the variability of crack initiation sites.

This behaviour highlights a critical limitation of purely geometrical interpretations of surface roughness. Although chemical milling reduces global roughness parameters, it does not necessarily mitigate fatigue-related defect severity. Instead, it may increase the sharpness and irregularity of near-surface discontinuities, especially in precipitate-rich regions formed during ageing. As a consequence, fatigue performance cannot be reliably predicted from average roughness values alone; it requires consideration of local defect morphology and subsurface integrity.

The use of geometrical stress-concentration models, such as the Arola–Williams [81] approach and the Murakami framework, provides a functional engineering-level interpretation of these effects; however, their application to additively manufactured

surfaces should be regarded as an approximation. The complex, multi-scale nature of AM surface features and the interaction with residual stress fields introduce deviations from the idealised defect geometries assumed by these models. Despite these limitations, the convergence between fractographic observations, defect-severity metrics and fatigue results supports the proposed interpretation.

Finally, the markedly increased scatter observed in the aged and chemically milled condition is particularly relevant from an industrial perspective, as it reflects a reduced predictability of fatigue life rather than a simple reduction in the mean endurance limit. This aspect is especially critical for fatigue-critical components, where reliability and consistency are often more important than peak performance.

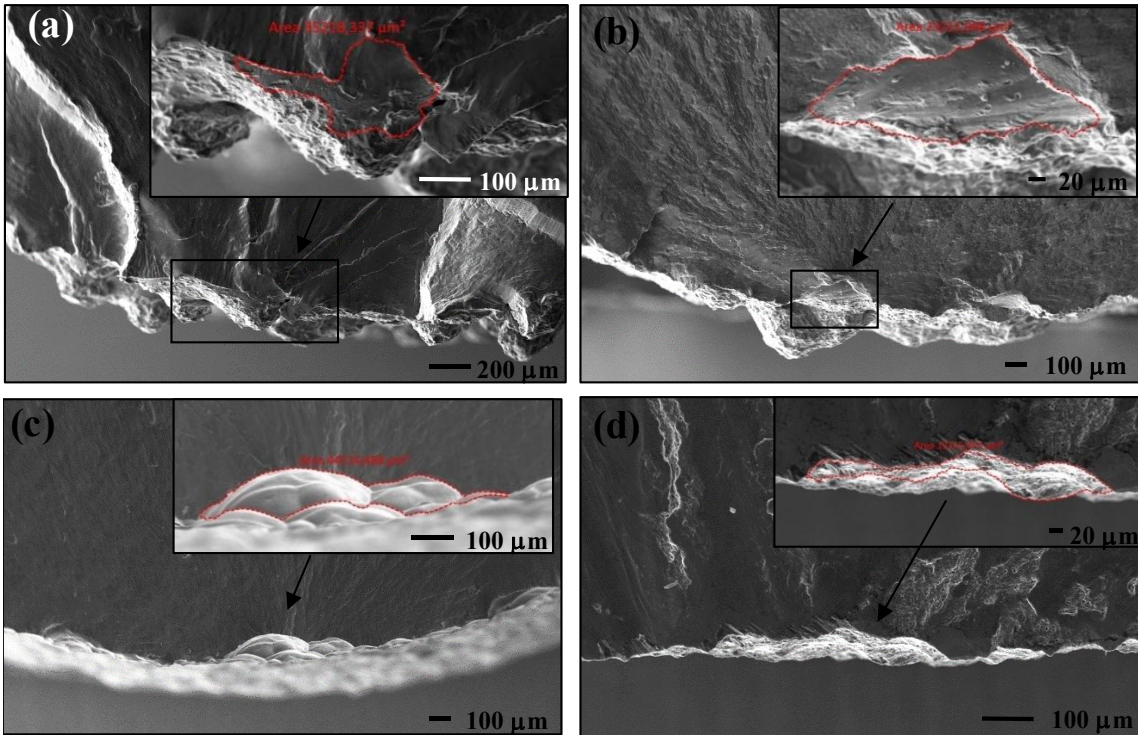

Figure 16 - SE-SEM micrographs of representative fracture surfaces following fatigue tests performed at 120 MPa for sandblasted specimens and 80 MPa for chemically milled ones.

Figure 16 provides SE-SEM micrographs of representative fracture surfaces. Sandblasted specimens (Figure 16a), both in the stress-relieved and aged conditions (Figure 16b), show that the fracture origin is typically located along a roughened surface ridge, where the crack initiates at a geometrical discontinuity produced by sandblasting. The crack initiation area in a sandblasted and aged specimen (Figure 16b) is similar to that found in the specimen subjected only to sandblasting. In this case, the crack also initiates at a geometrical discontinuity along a roughened surface ridge. However, the crack front appears sharp and well-defined. The crack initiation in this specimen is governed by the

geometrical discontinuities generated by sandblasting, which create sharp asperities acting as effective stress concentrators. Although ageing stabilizes the microstructure, the mechanically induced surface features primarily dictate the initiation mechanism in this condition [82, 83]. These observations reinforce the correlation between post-processing strategy and fatigue performance, confirming that surface condition plays a decisive role in determining the location, shape, and severity of fracture initiation sites in L-PBF AlSi10Mg alloys. In chemically milled specimens (Figures 16c and 16d), higher mean brightness and lower edge density are observed compared to sandblasted specimens (Figures 16a and 16b). In the chemically milled specimen not subjected to prior ageing, the crack originates at the outer surface in correspondence with an etched cavity, where multiple partially fused particles and morphological discontinuities are evident (Figure 16c). The crack front appears relatively smooth and uniform, consistent with the low edge-density values obtained from image analysis [84, 85]. The aged specimens treated by chemical milling exhibited the highest edge density values, as visible in Figure 16d. In contrast to the specimen subjected only to chemical milling, the crack front is highly irregular and propagates from a rough-surface depression (Figure 16d). Additionally, this region appears wider, suggesting more fragmented and irregular crack-origin zones, likely due to the presence of etching-induced discontinuities. High-magnification SEM observations further reveal that the surfaces of aged and chemically milled specimens exhibit etched cavities and localised morphological discontinuities. These features indicate that the combined effect of thermal exposure (ageing) and chemical attack may have contributed to a more irregular morphology of crack initiation. While the evidence does not allow for a quantitative assessment of the extent of such effects, the observed surface relief is consistent with enhanced microstructural heterogeneity and localised stress-concentration sites, which could promote earlier crack initiation. These findings support the hypothesis that ageing influences not only the surface morphology, but also the subsurface stress distribution, thereby affecting the mechanisms governing fatigue crack initiation in L-PBF AlSi10Mg alloys [83, 86, 87]. To complement the fractographic observations, the severity of surface defects was quantified using the geometrical stress concentration factor Kt according to the Arola Williams model, given by:

$$K_t = 1 + 2\sqrt{\frac{a}{\rho}}$$

where '*a*' is the defect depth estimated from 3D profilometry, and ρ is the local radius of curvature measured from SEM profiles. The corresponding fatigue notch factor k_f was obtained using the Peterson relation:

$$k_f = \frac{1}{1 + \frac{a_0}{\rho}} K_t$$

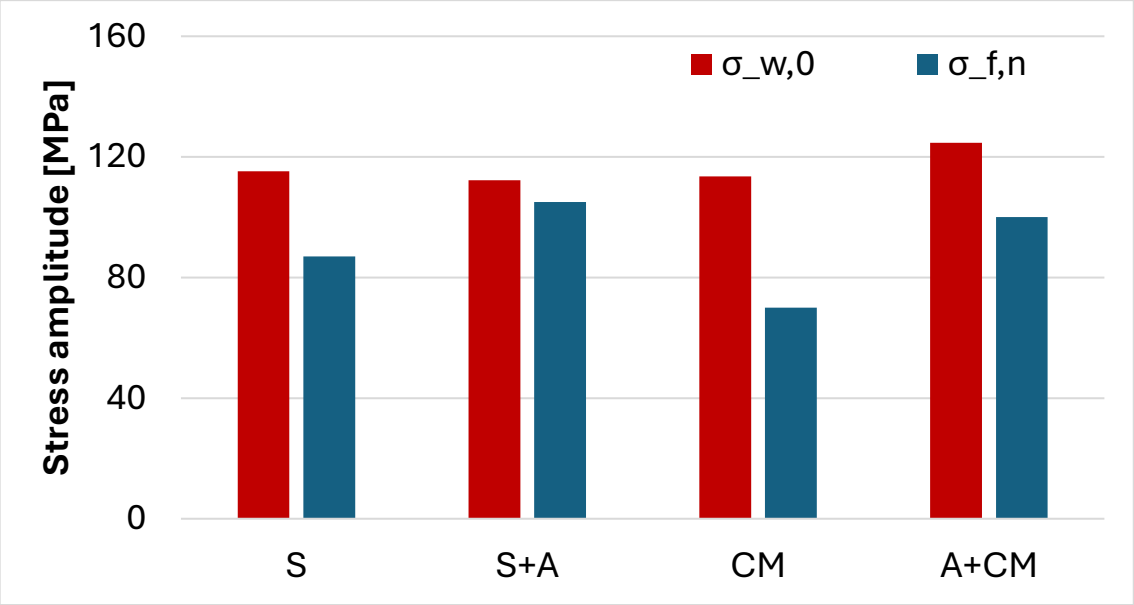

Figure 17 - Comparison between the local fatigue limit $\sigma_{w,loc}$, and the nominal fatigue strength $\sigma_{f,n}$ evaluated at N=3·10^6 cycles (50% survival probability) for all tested specimens under the four surface conditions.

A nominal fatigue limit $\sigma_{w,loc} = 120$ MPa, corresponding to the sandblasted and aged condition, was adopted as a smooth-reference baseline for Murakami's approach. This value was kept constant for all surface conditions to quantify the relative reduction of local fatigue strength due to surface defects through the fatigue notch factor

$$K_f = \frac{\sigma_{w,0}}{\sigma_{w,loc}}$$

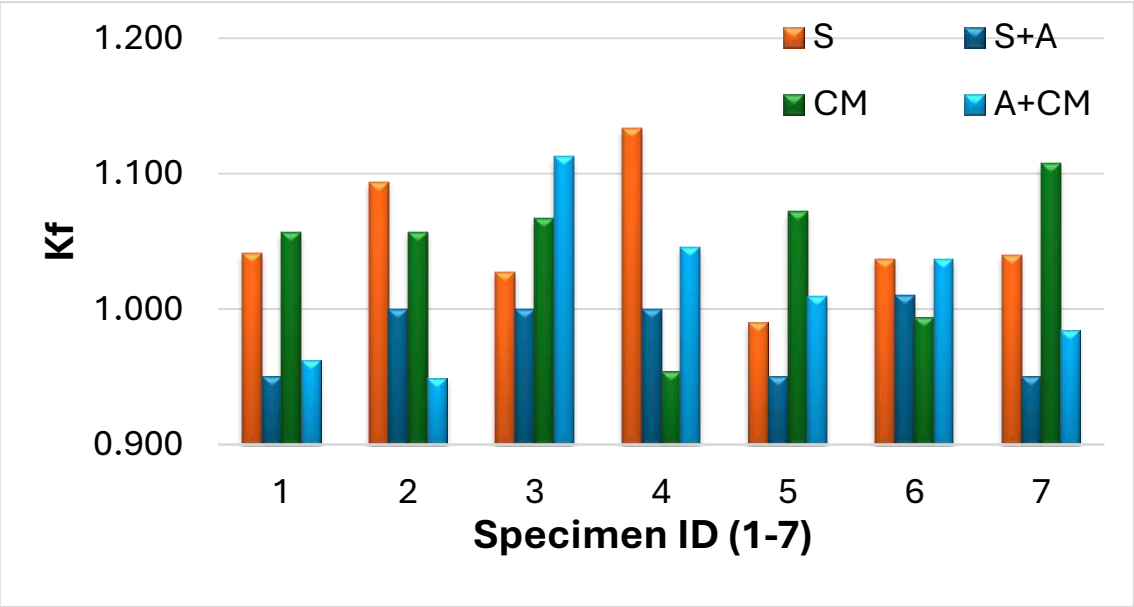

Figure 18 - Fatigue notch factor Kf calculated for all tested specimens under the four surface conditions. The x-axis reports specimen identifiers (1-7) and does not represent a physical variable.

This quantitative analysis further confirmed the experimental trends. Sandblasted specimens exhibited the lowest defect severity (Kt = 1.79, Kf = 1.21), which is consistent with their smoother crack-initiation sites and higher endurance limit. Chemically milled samples showed markedly sharper and deeper surface discontinuities, leading to significantly higher stress concentration factors (CM: Kt = 3.37, A+CM: Kt = 4.47). The corresponding reduction in the estimated fatigue limit matched the experimentally observed ordering of fatigue resistance. The Murakami approach further supported this interpretation. Using the $\sqrt{area}$ parameter extracted from SEM crack-initiation contours, the predicted endurance limits decreased from approximately 116 MPa (S) to 85–92 MPa (CM and A+CM), aligning with the S–N data. This combined analytical framework quantitatively explains why chemical milling, particularly when applied after ageing, amplifies near-surface discontinuities and reduces fatigue resistance.

Chapter 4 – Field assisted powder upcycling: Spark Plasma Sintering (SPS)

4.1 Introduction to SPS technology

Spark Plasma Sintering, also widely recognised as the Field Assisted Sintering Technique or Pulsed Electric Current Sintering, is a transformative advanced sintering method that synergistically combines pulsed direct current with uniaxial pressure [88, 89, 90, 91] . This sophisticated technique is designed to consolidate powdered materials into high-density bulk components rapidly, setting it apart from conventional sintering processes by achieving accelerated densification kinetics at significantly lower processing temperatures and in substantially shorter durations [88, 89, 90, 92, 93].

The operational principle of SPS is Joule heating, in which a pulsed DC is passed through electrically conductive powder compacts and/or the surrounding graphite tooling [93, 94]. This internal generation of heat, alongside the external mechanical pressure, drives the densification process [93, 94]. In electrically conductive powders, current flows through the particles, generating heat directly at the contact points. In instances where the powder compact is non-conductive, the heat is primarily generated by the resistive heating of the highly conductive graphite dies and plungers, which then efficiently transfers this thermal energy to the sample [88, 94]. This rapid and localised heating, often reaching rates exceeding several hundreds of degrees Celsius per minute (e.g., up to 1000 K/min), is a hallmark of SPS, minimising thermal gradients within the sample and allowing for precise control over the sintering profile [89, 90]. Consequently, the typical processing time in SPS is drastically reduced to minutes, a stark contrast to the hours often required by conventional hot pressing or pressure less sintering methods [89, 90].

A paramount advantage of SPS is its capacity to achieve high relative densities, frequently approaching theoretical maximums, while simultaneously suppressing undesirable grain growth [89, 90]. The rapid heating and short holding times characteristic of SPS limit the time available for grain boundary migration, thereby preserving fine-grained or even nanocrystalline microstructures [88, 89, 90, 95]. The preservation of such fine microstructures is highly desirable as it often translates into superior mechanical properties, including enhanced hardness, strength, fracture

toughness, and wear resistance [93]. This improved microstructural control positions SPS as an optimal method for fabricating refractory alloys and composites that demand high density and fine microstructures [95].

The precise densification mechanisms at play during SPS are multifaceted and continue to be a subject of in-depth scientific inquiry, involving a synergistic interplay of thermal, electrical, and mechanical factors [93, 94]. These mechanisms are generally understood to encompass plastic deformation under the applied uniaxial pressure, enhanced diffusion kinetics influenced by the electric field (electromigration), localised Joule heating at inter-particle contacts, and the presumed effect of plasma or spark discharges occurring at the particle boundaries [91, 96]. The pulsed nature of the electric current is thought to induce transient localised sparks or discharges between powder particles, which can effectively cleanse particle surfaces by breaking down oxide layers and other contaminants [96]. This "cleaning" action, along with the electric field, promotes improved inter-particle bonding and facilitates efficient mass transport, accelerating the densification process [97].

SPS technology has demonstrated remarkable versatility, successfully consolidating an extensive array of advanced materials across various domains [92, 93, 98, 99]. Its ability to fabricate materials with tailored microstructures and exceptional densities makes it particularly valuable for processing high-melting point materials, intricate compositions, and those requiring specific microstructural architectures for optimised functional performance [91, 92, 95]. Notable applications include the fabrication of advanced ceramics, magnetic materials, intermetallics, metallic glasses, high entropy alloys, and a wide variety of composites [92, 93, 99]. Furthermore, SPS is a preferred method for consolidating nanocrystalline and amorphous powders, where the retention of fine grain sizes is crucial for exploiting their unique properties [88, 100]. The ability to precisely control sintering parameters in SPS allows for the strategic tailoring of microstructures to achieve specific functional properties, which is critical for developing high-performance components in sectors ranging from space science and aeronautics to automation, mechanical engineering, and biomedicine [98]. The continuous evolution of SPS, including developments such as ultrahigh-pressure SPS, continues to expand its capabilities and applications, offering new possibilities for synthesizing and exploring novel materials [88, 91].

4.2 Two seemingly distant processes, a common underlying issue

The comprehensive study of fatigue resistance in L-PBF AlSi10Mg has unequivocally demonstrated that the cyclic performance of an additively manufactured component is profoundly influenced by its surface condition. Even when bulk material exhibits exceptionally high densities, approaching 99.5% global porosity, with defects predominantly subsurface or of minimal scale, the mechanical behaviour under cyclic loading remains critically dominated by the intricate characteristics of the surface. This includes asperities, irregularities stemming from laser scan paths or subsequent post-processing operations, and chemical-morphological discontinuities introduced by various surface treatments. The detailed analyses conducted across the sandblasted (S), sandblasted and aged (S+A), chemically milled, and aged and chemically milled (A+CM) conditions consistently revealed that even a perfectly dense material can experience premature fatigue failure if its surface harbours critical morphologies capable of locally amplifying applied stresses. Conversely, surfaces rendered uniform and refined through controlled mechanical treatments can significantly elevate the material's fatigue endurance, simultaneously reducing the dispersion of results and stabilising the mechanisms of crack initiation. This highlights the crucial role of surface quality in dictating the overall fatigue life and reliability of additively manufactured components.

This paramount importance of the surface is not merely a technical observation; it also serves as a symptom of a systemic limitation inherent in laser fusion additive processes. The entire Laser Powder Bed Fusion process is inherently energy-intensive, requiring meticulous control over the process atmosphere and demanding significant thermal management during fabrication. Furthermore, despite its apparent efficiency in material usage during the build, the process regrettably generates non-negligible volumes of exhausted powder. This exhausted powder is frequently deemed unsuitable for subsequent printing cycles due to alterations in melt pool stability, absorption of atmospheric oxygen, and undesirable changes in its granulometric distribution [50]. Consequently, the additive manufacturing supply chain often produces a residual material that cannot be easily reintroduced into the primary printing process, thereby posing a concrete and significant limitation to its overall sustainability [43].

In this specific context, the experimental results obtained through Spark Plasma Sintering on recycled powders unveil a radically different and highly promising technological scenario. Here, powder originally deemed unsuitable for direct L-PBF due to property

degradation is not merely discarded. Instead, it is transformed into a new, advanced material, endowed with superior mechanical properties and a more stable microstructure [88, 93]. While Laser Powder Bed Fusion and Spark Plasma Sintering are fundamentally distinct processes, their conceptual integration allows for a revolutionary rethinking of the entire lifecycle of metallic powders. This synergistic approach introduces innovative upcycling pathways that effectively circumvent the inherent limitations of laser fusion and compensate for its structural material waste [101, 102]. By combining the geometric flexibility of AM with the superior consolidation capabilities and microstructure control offered by SPS, it becomes possible to create components with enhanced properties from otherwise unusable material, thus addressing critical sustainability concerns in advanced manufacturing.

4.3 Exhausted Powder: a constraint and an opportunity

Throughout additive manufacturing cycles, the metallic powder feedstock undergoes a progressive and inevitable deterioration. This degradation manifests in several critical ways: the oxygen content within the powder increases, particle shape and granulometric distribution are altered, powder flowability diminishes, and the presence of moisture or oxide films can significantly interfere with the stability of the melt pool during the Laser Powder Bed Fusion process [103, 104]. For these cumulative reasons, return powder that has been exposed to multiple build cycles is typically classified as "out of specification" and subsequently set aside. Key challenges associated with powder recycling include maintaining consistent particle size and shape, managing contamination, and mitigating degradation effects from repeated use, such as wear, fragmentation, and oxidation [105].

This accumulation of unusable powder presents a significant paradox within the context of Additive Manufacturing, a technology frequently championed for its efficiency and sustainable potential. A non-negligible portion of the initial material – which is often expensive and produced through energy-intensive processes – ultimately becomes unsuitable for further use in the primary L-PBF process. This generates a material residue that is not easily reintroducible into the additive process, thereby posing a concrete and significant limitation to the purported sustainability benefits of AM [105, 106]. While the non-solidified powder material can often be recycled, its properties can change, influencing the resource efficiency of the process [107, 108].

However, the analysis conducted through Spark Plasma Sintering in this study reveals a radically different approach to understanding and valorising this otherwise exhausted powder. Rather than reintroducing the degraded powder into the fusion process, the SPS approach transforms it into a new, viable feedstock for high-energy powder metallurgy. This method offers an alternative to conventional additive [102] manufacturing approaches by reducing the time and temperature required for densification [102]. The mechanical alloying process employed in the SPS work completely obliterates the original geometric characteristics of the powder particles, instead promoting the thorough mixing of various elemental components. Simultaneously, it strategically leverages elements such as oxygen and carbon, often released by processing control agents, to control the formation of advanced ceramic phases within the consolidated material. This approach allows for rapid prototyping of complex metal and ceramic structures with high material flexibility and low environmental impact [102].

This conceptual shift is crucial: what constitutes a significant problem in L-PBF – namely, powder oxidation, granulometric ageing, and the loss of particle sphericity – becomes a distinct advantage in the SPS process. These "detrimental" characteristics actively fuel the nucleation and growth of beneficial oxides and carbides, which are instrumental in consolidating a high-performance composite material [109, 110]. Consequently, oxygen is no longer viewed solely as a contaminant to be meticulously reduced; instead, it is utilised as a vital component for the deliberate synthesis of phases such as chromium oxide (Cr_2O_3). Similarly, the carbon introduced, for instance, by the PCA, is not merely an impurity but rather forms the foundational basis for the creation of high-strength phases like niobium carbide and chromium carbide (Cr_7C_3) [111]. This transformative approach not only mitigates waste but also opens new avenues for material design and performance enhancement through strategic upcycling.

4.4 The role of Spark Plasma Sintering in L-PBF powder upcycling

The Spark Plasma Sintering of the $CoCrFeNiMo_xNb_{0.4x}$ material, as demonstrated in this study, reveals a fundamentally different dynamic compared to that observed in Laser Powder Bed Fusion processes. The combined application of pulsed electric current and uniaxial pressure within SPS induces extremely rapid heating, enabling the efficient

consolidation of powdered materials within mere minutes and at significantly moderate temperatures [88, 89, 90, 93]. This rapid processing sets SPS apart from conventional methods and offers unique advantages for material synthesis.

In the subsequent stage, the pre-alloyed powder exhibits a characteristic lamellar structure. This morphology is typical of materials processed via mechanical alloying, featuring zones enriched in nickel, niobium, and molybdenum, which are inherited from the Inconel waste components. Alongside these, regions rich in iron and chromium are also present, resulting from partial elemental segregation during mechanical alloying. This initial heterogeneous state of the powder highlights the challenge of using recycled materials, yet also presents an opportunity when processed correctly.

During the SPS process, these elemental and microstructural differences are largely mitigated and overcome through intense diffusive processes. Rapid heating and pressure facilitate atomic mobility, leading to the stabilisation of a continuous face-centred cubic (fcc) metallic matrix. Concurrently, the method enables controlled nucleation and growth of specific ceramic phases within this matrix. The formation of compounds such as chromium oxide (Cr2O3), chromium carbide (Cr7C3), and niobium carbide is not merely a side effect; rather, it is a constitutive feature of the newly formed material. These ceramic phases play a crucial role, acting as effective dispersion strengtheners within the metallic matrix [109, 110].

The outcome of this transformative process is a nano-reinforced metallic matrix that exhibits significantly higher thermal stability than conventional non-composite fcc alloys. The presence of these finely distributed ceramic particles creates a strong pinning effect, effectively hindering grain growth even at elevated temperatures [95]. This suppression of grain coarsening is critical for maintaining superior mechanical properties, as fine-grained microstructures generally correlate with enhanced strength and hardness. This unique microstructural architecture, characterised by a refined matrix and uniformly dispersed strengthening phases, contributes directly to the improved performance of the upcycled material.

What makes this result particularly significant from a sustainability and materials science perspective is that these enhanced properties do not necessitate the use of high-quality, virgin primary powders. On the contrary, the very presence of elements derived from the degradation of the Inconel powder – such as oxides, variations in elemental composition,

and micro-fragmentations – actively contributes to the formation and refinement of the final material. The process effectively re-engineers what would otherwise be considered defects into beneficial microstructural features [111].

This observation is fundamental for fostering greater sustainability in additive manufacturing. The material obtained through SPS is not merely produced "despite" the use of discarded powder; instead, its superior characteristics are achieved precisely "because" of it. This represents a clear and compelling case of upcycling, where what was once a waste material is valorised into a product possessing superior performance and value compared to its original, primary feedstock. This innovative approach to material processing offers a pathway to significantly reduce waste, enhance material efficiency, and unlock new possibilities for high-performance applications using previously unusable resources, directly addressing the systemic limitations of powder management in L-PBF.

4.5 Convergences and divergences between L-PBF and SPS

A comparative analysis of Laser Powder Bed Fusion and Spark Plasma Sintering reveals two fundamental distinctions in their operational principles and, consequently, their impact on material properties. In L-PBF, the surface emerges as the truly critical element dictating mechanical behaviour. The selective fusion process inherently generates layer asperities, localised folds, potential micro-cracks, and microstructural inhomogeneities on the surface. These features necessitate intensive post-processing treatments that, even then, often cannot eliminate these defects without introducing additional collateral effects. Consequently, the fatigue life of the material produced via L-PBF is primarily governed by the intricate control of surface topography and the mitigation of stress-concentrating features [82, 83, 86]. Even with high bulk densities and minimal internal defects, critical surface morphologies can locally amplify stresses, leading to premature failure [4]. Conversely, uniform surfaces achieved through controlled mechanical treatments like sandblasting can significantly elevate the material's fatigue endurance, reducing data scatter and stabilising crack initiation mechanisms [86].

In stark contrast, within the SPS process, the surface does not play the same dominant role. Morphological defects in SPS components do not originate from a layer-by-layer fusion process within a powder bed. Instead, consolidation occurs through a quasi-

isostatic process where electrical and mechanical energy are uniformly distributed throughout the powder compact [88, 89, 90, 93]. In SPS, the internal microstructure, specifically governed by the nanometric distribution of ceramic phases, becomes the primary determinant of mechanical performance. The resulting properties do not rely on surface optimisation in the same way as L-PBF; rather, they are a direct outcome of the synergistic control between the metallic matrix and the strategically dispersed strengthening phases [109, 110]. This fundamental difference highlights a shift from external surface control to internal microstructural design as the key to achieving desired mechanical properties.

From this comparative perspective, a broader model of sustainability clearly emerges. L-PBF remains an indispensable technology for the production of complex geometries and lightweight components, offering unparalleled design freedom [5]. However, a significant drawback is its generation of non-negligible quantities of exhausted powder that the technology itself cannot effectively reabsorb [43, 103, 104]. This constitutes a substantial material waste stream and a limitation to L-PBF's sustainability claims [105, 106]. SPS, on the other hand, offers a transformative solution by enabling the upcycling of this very same exhausted powder. It transforms what would otherwise be considered waste into an advanced material, suitable for compact components, structural inserts, or functional elements where high mechanical performance and thermal stability are critical [101, 102, 111].

This integration fundamentally redefines the lifecycle of additive manufacturing powders. The traditional linear progression (virgin powder → print → waste) is replaced by a more sustainable circular economy model (virgin powder → print → exhausted powder → advanced material via SPS). This innovative approach not only mitigates the environmental impact associated with material waste in L-PBF but also unlocks new potential for creating high-performance materials from a previously undervalued resource, thereby significantly enhancing the overall sustainability of advanced manufacturing processes.

Chapter 5 – General Discussion

5.1 Summary of results

This study rigorously investigated the intricate relationship between various post-processing treatments, the resulting surface morphology, and the fatigue properties of L-PBF AlSi10Mg alloys. The findings unequivocally demonstrate a clear and significant correlation between the chosen post-processing techniques and the fatigue life of these additively manufactured components. While additive manufacturing offers unprecedented capabilities in terms of geometric complexity and reduced lead times, the inherent characteristics of as-built parts, such as surface roughness and process-induced defects, often necessitate subsequent post-processing to achieve mechanical properties comparable to, or even surpassing, those of conventionally manufactured materials [4, 112].

Sandblasting, a mechanical surface treatment, was shown to produce finer, more uniformly distributed surface textures generally. This leads to enhanced fatigue resistance, primarily by introducing compressive residual stresses and by smoothing critical surface imperfections that could act as stress concentrators. Conversely, chemical milling, a subtractive process, modifies the near-surface morphology more aggressively by removing material through selective chemical dissolution. The precise outcome of chemical milling depends heavily on the initial surface state and, crucially, on the material's microstructural characteristics. When chemical milling is applied after an ageing heat treatment, the resulting surface relief is a complex interplay between the chemical etching action and the underlying microstructural state altered by the ageing process. In the present study, specimens that underwent ageing followed by chemical milling (A+CM) exhibited higher fatigue resistance than those treated with chemical milling alone. This critical observation highlights that the sequence of treatments, rather than chemical milling in isolation, plays a pivotal role in determining the final fatigue behaviour. These fundamental modifications to the surface directly impact the mechanisms governing fatigue crack initiation. The underlying microstructure of the AlSi10Mg alloy, particularly its homogeneity and secondary phase distribution, plays a crucial role in determining its overall fatigue behaviour [87]. The ageing process contributes to homogenising the microstructure, reducing directional solidification patterns, and improving the distribution of silicon precipitates. These microstructural

refinements are known to enhance fatigue properties [113]. However, an aggressive chemical milling process, such as that employed in this study, can potentially negate these beneficial microstructural improvements. This is primarily due to preferential etching of precipitate-rich zones, leading to more fragmented, irregular crack-origin zones at the surface.

Furthermore, porosity and other inherent defects arising from the L-PBF process can significantly compromise the fatigue performance of components [113, 114]. These defects, whether they are small lack-of-fusion pores or gas inclusions, act as potent stress concentrators, thereby facilitating the initiation and subsequent propagation of fatigue cracks. Consequently, the fatigue properties of additively manufactured parts are highly dependent on the nature and distribution of these defects, the surface quality, and the presence of residual stresses [113, 114]. The manufacturing process often favours the formation of gas pores and lack-of-fusion inclusions, both of which can significantly influence mechanical properties and must therefore be meticulously avoided or at least minimised during fabrication. The inherent diversity and complex shapes of defects in AM components, which can differ significantly from those in conventionally produced components, necessitate specialised characterisation techniques for accurate fatigue-life prediction [115]. The challenge of accurately predicting fatigue life in L-PBF materials is substantial, primarily due to various process-induced effects, including microstructural inhomogeneities, surface roughness, material anisotropy, and residual stresses [4]. Moreover, the as-built state of AM parts poses considerable challenges, with the surface texture often serving as primary nucleation sites for fatigue cracking. This, coupled with residual thermal stresses or suboptimal microstructures, can significantly reduce overall fatigue lifetimes. The well-documented benefits of sandblasting in improving surface finish and, consequently, fatigue life are consistent with these findings [86]. Similarly, the detrimental effects of chemical milling on fatigue performance, particularly when microstructural defects are present, have been previously reported.

However, this study is subject to certain limitations that warrant consideration for future research. The fatigue-testing sample size was limited, which may affect the statistical significance and generalizability of the results. Future research endeavours should therefore focus on expanding the sample population to bolster statistical robustness. Additionally, optimising post-processing strategies to achieve an optimal balance between mechanical integrity and surface quality in AM components remains a critical

area for investigation. This includes exploring alternative surface-finishing techniques, such as laser polishing, which offers precise material removal, as well as refining the intensity and parameters of currently applied processes, such as microwave-assisted chemical milling. Further research is also needed to investigate the effects of different heat-treatment parameters on both microstructural evolution and fatigue performance. Ultimately, the development of robust predictive models that can accurately forecast the fatigue life of AM components based on their complex microstructure, inherent defect characteristics, and anticipated loading conditions will be essential for the widespread industrial adoption of these advanced materials.

5.2 Future research directions

Future research stemming from this thesis will focus on extending the present analysis both in terms of processing routes and material systems, with the objective of consolidating the generality of the observed fatigue mechanisms. A first research direction concerns the further investigation of Spark Plasma Sintering (SPS) as an alternative powder consolidation technique. Compared to Laser Powder Bed Fusion, SPS is characterised by fundamentally different thermal and kinetic conditions, including rapid heating rates, limited exposure to high temperatures and reduced interaction with the surrounding atmosphere. Building on the preliminary considerations discussed in this work, future studies will aim to systematically compare SPS-processed and L-PBF components in terms of microstructural stability, defect population and fatigue behaviour. Particular attention will be devoted to the role of powder reuse and oxygen uptake, in order to assess whether SPS can shift the fatigue-controlling mechanisms from surface-dominated to bulk-dominated regimes.

A second research direction involves extending fatigue investigations to AISI 316L stainless steel and titanium alloys, which represent technologically relevant materials with markedly different microstructural characteristics and deformation mechanisms compared to AlSi10Mg. These materials exhibit different sensitivities to surface condition, residual stresses and internal defects, and therefore provide an appropriate framework to test the transferability of the conclusions drawn in this thesis. Future work will address high-cycle fatigue behaviour under controlled post-processing conditions, with the aim of identifying common trends and material-specific deviations in crack

initiation mechanisms. This comparative approach is expected to contribute to a more general framework for fatigue assessment in additively manufactured metallic materials.

5.3 Scientific and industrial contribution

From a scientific standpoint, this thesis contributes to the current understanding of fatigue behaviour in additively manufactured metals by demonstrating that fatigue performance is not solely determined by the final surface condition, but is strongly influenced by the processing history and the sequence of post-processing treatments. Through an integrated analysis combining fatigue testing, surface and microstructural characterisation, and defect-based modelling approaches, the work provides mechanistic insight into the role of near-surface features and their interaction with thermal history in governing crack initiation and fatigue-life scatter. The results highlight the limitations of global roughness descriptors and support the adoption of local, defect-oriented metrics for the interpretation and prediction of fatigue behaviour in additively manufactured components.

In addition to its scientific contribution, the thesis is relevant to industrial research contexts, particularly within Tetra Pak, where additive manufacturing is being explored for the development of components and tooling subjected to cyclic loading. The findings provide a knowledge base for the rational selection of post-processing strategies and material systems, supporting the qualification of additively manufactured parts in applications requiring high reliability. More broadly, the methodologies and conceptual framework developed in this work apply to a wide range of additively manufactured metals and help bridge the gap between experimental fatigue characterisation and the practical deployment of additive manufacturing technologies in engineering systems.

Conclusion

This comprehensive study meticulously investigated the profound impact of various post-processing techniques – specifically sandblasting, chemical milling, and their integration with T6 heat treatment – on the fatigue behaviour of L-PBF AlSi10Mg alloy. The findings unequivocally demonstrate that the choice of post-processing methods, and crucially their sequential application, significantly influences the resulting surface morphology, the underlying microstructure, and ultimately the fatigue life of the material. This research provides critical insights to advance the reliability and performance of additively manufactured components in demanding engineering applications.

The mechanical surface modification imparted by sandblasting was shown to produce a more homogeneous yet relatively rough surface topography. This consistent surface condition contributed to a stable and often improved fatigue response, primarily by introducing beneficial compressive residual stresses and smoothing localised imperfections that act as stress concentrators. In contrast, chemical milling, through its mechanism of selective chemical dissolution, effectively reduces surface height variations and can achieve a smoother surface finish. However, the precise interaction of chemical milling with the material's microstructure proved to be a critical determinant of fatigue performance. A key finding was that specimens subjected to an ageing treatment followed by chemical milling (A+CM) exhibited notably higher fatigue resistance compared to those treated with chemical milling alone. This highlights that the sequence of thermal and chemical treatments, rather than the chemical process alone, plays a pivotal role in determining the final surface condition and its corresponding fatigue behaviour. The T6 heat treatment, by inducing microstructural homogenisation and altering the distribution of silicon precipitates, fundamentally alters the material's internal state, thereby influencing how subsequent surface treatments interact with it.

The study strongly emphasises that the fatigue response of L-PBF AlSi10Mg components is predominantly controlled by the inherent defect population within the material, particularly the characteristics of surface defects and microstructural discontinuities. These imperfections act as critical initiation sites for fatigue cracks, thereby governing the overall fatigue life. Quantitative analyses, including the application of the Arola Williams model for geometrical stress concentration factors and the Murakami approach, corroborated these experimental observations. These models demonstrated that

sandblasted surfaces, by reducing defect severity, significantly improved the fatigue notch factor and, consequently, the endurance limit. Conversely, chemical milling, especially when applied after ageing, was shown to amplify near-surface discontinuities, leading to higher stress concentration factors and a corresponding reduction in fatigue resistance. The implications of this research are significant for the design and manufacturing of fatigue-critical components made from the L-PBF AlSi10Mg alloy. The insights from this study can guide the development of optimised post-processing strategies for AM components, thereby improving reliability and performance in engineering applications. Further research could focus on optimising post-processing strategies to balance mechanical integrity and surface quality in AM components.

Beyond the immediate findings on L-PBF AlSi10Mg fatigue, the combination of two seemingly distant research lines – one focused on L-PBF component fatigue and the other on Spark Plasma Sintering of recycled powders – allows for the articulation of a new vision for the entire additive manufacturing supply chain. It is not realistic to assume that the sustainability of a single process can be achieved solely by reducing internal waste. Instead, it is imperative to reconsider the entire lifecycle of metallic powders and integrate complementary technologies that can valorise what L-PBF processes cannot reuse. The L-PBF process, while revolutionary for complex geometries, generates exhausted powder that cannot be reabsorbed into its own cycle, posing a significant waste challenge [43, 105].

In this broader perspective, SPS emerges as a pivotal technology capable of transforming a problematic residue into a valuable resource. By utilising exhausted L-PBF powders, SPS can produce highly stable, nano reinforced, advanced materials with composite microstructures suitable for applications where mechanical strength and thermal stability are critical [88, 93, 109, 110]. This approach leverages the very characteristics of degraded Inconel powder – such as oxides, compositional variations, and micro-fragmentations – as beneficial elements that contribute to the formation of high-performance composites, like those with Cr_2O_3, Cr_7C_3, and NbC phases [102, 111]. The joint analysis of these two distinct studies unequivocally demonstrates that achieving sustainability in Additive Manufacturing is not an incremental goal, but rather a process of technological integration. Only by incorporating tools that can give new life to exhausted materials can we create truly circular supply chains and significantly reduce reliance on virgin primary powders. This paradigm shift from a linear powder cycle

(powder → print → waste) to a circular one (powder → print → waste → advanced material via SPS) represents a fundamental step towards a more sustainable future for advanced manufacturing.

References

[1] Costa, J., Sequeiros, E. W., Figueiredo, D., Reis, A., & Vieira, M. F. (2024). Optimizing Metal AM Potential through DfAM: Design, Performance, and Industrial Impact. In *IntechOpen eBooks*. IntechOpen. https://doi.org/10.5772/intechopen.1007309

[2] Kirihara, S., & Nakata, K. (2020). Multi-dimensional Additive Manufacturing. In *Springer eBooks*. Springer Nature. https://doi.org/10.1007/978-981-15-7910-3

[3] Reintjes, C. (2022). Algorithm-Driven Truss Topology Optimisation for Additive Manufacturing. In *Springer eBooks*. Springer Nature. https://doi.org/10.1007/978-3-658-36211-9

[4] Strauß, L., Duarte, L., Kruse, J., Madia, M., & Löwisch, G. (2025). An equivalent stress approach for predicting fatigue behaviour of additively manufactured AlSi10Mg. *Progress in Additive Manufacturing*. https://doi.org/10.1007/s40964-025-00974-0

[5] Khan, M. A., & Jappes, J. T. W. (2022). Innovations in Additive Manufacturing. In *Springer tracts in additive manufacturing*. Springer International Publishing. https://doi.org/10.1007/978-3-030-89401-6

[6] Ghazali, M. I. M., Baharuddin, A. S., Alauddin, M. S., Dahlan, A., Fuzi, S. F. Z., Shaarani, S. M., & Hanafi, M. A. (2023). Additive manufacturing food: technology and materials. *Food Research*, *6*, 28. https://doi.org/10.26656/fr.2017.6(s3).009

[7] Padhiary, M., Barbhuiya, J. A., Roy, D., & Roy, P. (2024). 3D printing applications in smart farming and food processing. *Smart Agricultural Technology*, *9*, 100553. https://doi.org/10.1016/j.atech.2024.100553

[8] Escalante-Aburto, A., Santiago, G. T., Álvarez, M. M., & Chuck-Hernández, C. (2021). Advances and prospective applications of 3D food printing for health improvement and personalized nutrition [Review of *Advances and prospective applications of 3D food printing for health improvement and personalized nutrition*]. *Comprehensive Reviews in Food Science and Food Safety*, *20*(6), 5722. Wiley. https://doi.org/10.1111/1541-4337.12849

[9] Lipton, J., Cutler, M., Nigl, F., Cohen, D., & Lipson, H. (2015). Additive manufacturing for the food industry. *Trends in Food Science & Technology*, *43*(1), 114. https://doi.org/10.1016/j.tifs.2015.02.004

[10] Schiffer, Á., Sahai, N., & Ratnavel, S. (2024). *3D Printing Technologies and Automation in Food Processing Industry: An Innovative Marketing Approach for Health and Digital Gastronomy Perspective*. https://doi.org/10.26434/chemrxiv-2024-q37xr

[11] Colorado, H. A., Velásquez, E. I. G., & Monteiro, S. N. (2020). Sustainability of additive manufacturing: the circular economy of materials and environmental perspectives. *Journal of Materials Research and Technology*, *9*(4), 8221. https://doi.org/10.1016/j.jmrt.2020.04.062

[12] Sukindar, N. A., Noorazizi, M. S., Shaharuddin, S. I. Bt. S., Kamaruddin, S., Azhar, A. Z. A., Choong, Y. C., & Wahab, M. A. A. (2021). Implementation of 3D Printing Technology in the Food Industry. *Scientific Review*, *74*, 50. https://doi.org/10.32861/sr.74.50.54

[13] Estupiñán-López, F., Gaona-Tiburcio, C., Jáquez-Muñoz, J. M., Zambrano-Robledo, P., Maldonado-Bandala, E., Miramontes, J. Á. C., Nieves-Mendoza, D., Delgado, A. D., Ríos, J. P. F.-D. los, & Almeraya-Calderón, F. (2021). A Comparative Study of Corrosion AA6061 and AlSi10Mg Alloys Produced by Extruded and Additive Manufacturing. *Materials*, *14*(19), 5793. https://doi.org/10.3390/ma14195793

[14] Linder, C., Vucko, F., Ma, T., Proper, S., & Dartfeldt, E. (2023). Corrosion-Fatigue Performance of 3D-Printed (L-PBF) AlSi10Mg. *Materials*, *16*(17), 5964. https://doi.org/10.3390/ma16175964

[15] Costa, C. A., Luciano, M. A., & Pasa, A. M. (2013). Guiding Criteria for Hygienic Design of Food Industry Equipment. *Journal of Food Process Engineering*, *36*(6), 753. https://doi.org/10.1111/jfpe.12044

[16] Faille, C., Cunault, C., Dubois, T., & Bénézech, T. (2017). Hygienic design of food processing lines to mitigate the risk of bacterial food contamination with respect to environmental concerns.

Innovative Food Science & Emerging Technologies, *46*, 65. https://doi.org/10.1016/j.ifset.2017.10.002

[17] Hanisch, T., Stelzer, S. P., Eisenrauch, V., Milaev, N., Thielsch, J., Sebastian, J., Fuchs, E., & Mauermann, M. (2025). Influence of surface texture on the cleanability of 3D-printed stainless-steel components. *Heat and Mass Transfer*, *61*(9). https://doi.org/10.1007/s00231-025-03600-5

[18] Waldhans, C., Hebel, M., Herbert, U., Spoelstra, P., Barbut, S., & Kreyenschmidt, J. (2023). Microbial investigation of cleanability of different plastic and metal surfaces used by the food industry. *Journal of Food Science and Technology*, *60*(10), 2581. https://doi.org/10.1007/s13197-023-05778-0

[19] Alami, A. H., Olabi, A. G., Khuri, S., Aljaghoub, H., Alasad, S., Ramadan, M., & Abdelkareem, M. A. (2023). 3D printing in the food industry: Recent progress and role in achieving sustainable development goals. *Ain Shams Engineering Journal*, *15*(2), 102386. https://doi.org/10.1016/j.asej.2023.102386

[20] Déspeisse, M., & Ford, S. (2015). The Role of Additive Manufacturing in Improving Resource Efficiency and Sustainability. In *IFIP advances in information and communication technology* (p. 129). Springer Science+Business Media. https://doi.org/10.1007/978-3-319-22759-7_15

[21] Ghobadian, A., Talavera, I., Bhattacharya, A., Kumar, V., Garza-Reyes, J. A., & O'Regan, N. (2018). Examining legitimatisation of additive manufacturing in the interplay between innovation, lean manufacturing and sustainability. *International Journal of Production Economics*, *219*, 457. https://doi.org/10.1016/j.ijpe.2018.06.001

[22] Chua, C. K., Yeong, W. Y., & Wong, C. H. (2017). *Standards, quality control, and measurement sciences in 3D printing and additive manufacturing*. http://cds.cern.ch/record/2283957

[23] Pan, W., Ye, Z., Zhang, Y., Liu, Y., Liang, B., & Zhai, Z. (2022). Research on Microstructure and Properties of AlSi10Mg Fabricated by Selective Laser Melting. *Materials*, *15*(7), 2528. https://doi.org/10.3390/ma15072528

[24] Snopiński, P., Matus, K., & Hilšer, O. (2023). Investigation of the Effects of Various Severe Plastic Deformation Techniques on the Microstructure of Laser Powder Bed Fusion AlSi10Mg Alloy. *Materials*, *16*(23), 7418. https://doi.org/10.3390/ma16237418

[25] Macías, J. G. S., Douillard, T., Zhao, L., Maire, É., Pyka, G., & Simar, A. (2020). Influence on microstructure, strength and ductility of build platform temperature during laser powder bed fusion of AlSi10Mg. *Acta Materialia*, *201*, 231. https://doi.org/10.1016/j.actamat.2020.10.001

[26] Kobir, M. H., Yavari, R., Riensche, A., Bevans, B., Castro, L., Cole, K., & Rao, P. (2022). Prediction of recoater crash in laser powder bed fusion additive manufacturing using graph theory thermomechanical modeling. *Progress in Additive Manufacturing*, 8. https://doi.org/10.1007/s40964-022-00331-5

[27] Chen, L., Bi, G., Yao, X., Su, J., Tan, C., Feng, W., Benakis, M., Chew, Y., & Moon, S. K. (2024). In-situ process monitoring and adaptive quality enhancement in laser additive manufacturing: A critical review [Review of *In-situ process monitoring and adaptive quality enhancement in laser additive manufacturing: A critical review*]. *Journal of Manufacturing Systems*, *74*, 527. Elsevier BV. https://doi.org/10.1016/j.jmsy.2024.04.013

[28] Liu, Q., Wu, H., Paul, M. J., He, P., Peng, Z., Gludovatz, B., Kruzic, J. J., Wang, C., & Li, X. (2020). Machine-learning assisted laser powder bed fusion process optimisation for AlSi10Mg: New microstructure description indices and fracture mechanisms. *Acta Materialia*, *201*, 316. https://doi.org/10.1016/j.actamat.2020.10.010

[30] Huang, M., Yang, B., Zhou, Y., Guan, X., Wang, Y., Liao, Z., Xiao, S., Yang, G., & Zhu, T. (2024). Effect of Processing Parameters on Tensile Properties and Microstructure of Selective Laser Melted AlSi10Mg Alloy. *Journal of Materials Engineering and Performance*. https://doi.org/10.1007/s11665-024-09536-x

[31] Hendl, J., Marquardt, A., & Leyens, C. (2022). Electron beam powder bed fusion manufacturing of a Ti-5Al-5Mo-5V-3Cr alloy: a microstructure and mechanical properties' correlation study. *Progress in Additive Manufacturing*, *8*(3), 459. https://doi.org/10.1007/s40964-022-00338-y

[32] Krooß, P., Lauhoff, C., Gustmann, T., Gemming, T., Sobrero, C., Ewald, F., Brenne, F., Arold, T., Nematolahi, M., Elahinia, M., Thielsch, J., Hufenbach, J., & Niendorf, T. (2022). Additive Manufacturing of Binary Ni–Ti Shape Memory Alloys Using Electron Beam Powder Bed Fusion: Functional Reversibility Through Minor Alloy Modification and Carbide Formation. *Shape Memory and Superelasticity*, *8*(4), 452. https://doi.org/10.1007/s40830-022-00400-2

[33] Böhm, J., Breuning, C., Markl, M., & Körner, C. (2024). A new approach of preheating and powder sintering in electron beam powder bed fusion. *The International Journal of Advanced Manufacturing Technology*, *133*, 3769. https://doi.org/10.1007/s00170-024-13966-1

[34] Singh, S., Ramakrishna, S., & Singh, R. (2017). Material issues in additive manufacturing: A review. Journal of Manufacturing Processes, 25, 185–200. https://doi.org/10.1016/j.jmapro.2016.11.006

[35] Gong, X., Anderson, T. L., & Chou, K. (2014). Review on powder-based electron beam additive manufacturing technology. *Manufacturing Review*, *1*, 2. https://doi.org/10.1051/mfreview/2014001

[36] Philips, N., Rock, C., Cunningham, N. J., Cooper, J., & Horn, T. (2024). Electron Beam Powder Bed Fusion of ATI C103TM Refractory Alloy. *Metallurgical and Materials Transactions A*, *55*(7), 2472. https://doi.org/10.1007/s11661-024-07411-x

[37] Bian L., Thompson S. M., & Shamsaei N., Mechanical Properties and Microstructural Features of Direct Laser-Deposited Ti-6Al-4V, JOM, vol. 67, no. 3, pp. 629–638, 2015. https://doi.org/10.1007/s11837-015-1308-9

[38] Tzimanis, K., Koutsokeras, M. S., Bourlesas, N., Porevopoulos, N., Pastras, G., & Stavropoulos, P. (2025). Digital transformation of wire DED-LB: enabling industrial scalability through monitoring and control systems. *The International Journal of Advanced Manufacturing Technology*. https://doi.org/10.1007/s00170-025-16654-w

[39] Bayar, A., & Altuntaş, G. (2025). Effects of Thermal Spray Coatings on Surface Protection and Mechanical Performance of AlSi10Mg Alloy Produced by Additive Manufacturing. *DergiPark (Istanbul University)*. https://dergipark.org.tr/en/pub/gmbd/issue/94345/1661296

[40] Tradowsky, U., White, J., Ward, R., Read, N., Reimers, W., & Attallah, M. M. (2016). Selective laser melting of AlSi10Mg: Influence of post-processing on the microstructural and tensile properties development. *Materials & Design*, *105*, 212. https://doi.org/10.1016/j.matdes.2016.05.066

[41] Bisht, M. S., Gaur, V., & Singh, I. V. (2022). On mechanical properties of SLM Al–Si alloy: Role of heat treatment-induced evolution of silicon morphology. *Materials Science and Engineering A*, *858*, 144157. https://doi.org/10.1016/j.msea.2022.144157

[42] Padovano, E., Badini, C. F., Pantarelli, A., Gili, F., & D'Aiuto, F. (2020). A comparative study of the effects of thermal treatments on AlSi10Mg produced by laser powder bed fusion. *Journal of Alloys and Compounds*, *831*, 154822. https://doi.org/10.1016/j.jallcom.2020.154822

[43] Jung, S., Kara, L. B., Nie, Z., Simpson, T. W., & Whitefoot, K. S. (2023). Is Additive Manufacturing an Environmentally and Economically Preferred Alternative for Mass Production? [Review of *Is Additive Manufacturing an Environmentally and Economically Preferred Alternative for Mass Production?*]. *Environmental Science & Technology*, *57*(16), 6373. American Chemical Society. https://doi.org/10.1021/acs.est.2c04927

[44] Pusateri, V., Olsen, S. I., Kara, S., & Hauschild, M. Z. (2021). Life Cycle Assessment of metal additive manufacturing: a systematic literature review. *Research Portal Denmark*, *8*, 1. https://local.forskningsportal.dk/local/dki-cgi/ws/cris-link?src=dtu&id=dtu-410617eb-5296-406c-af58-8c56e8d4bf31&ti=Life%20Cycle%20Assessment%20of%20metal%20additive%20manufacturing%3A%20a%20systematic%20literature%20review

[45] Kokare, S., Oliveira, J. P., & Godina, R. (2023). Life cycle assessment of additive manufacturing processes: A review [Review of *Life cycle assessment of additive manufacturing processes: A review*]. *Journal of Manufacturing Systems*, *68*, 536. Elsevier BV. https://doi.org/10.1016/j.jmsy.2023.05.007

[46] Ochs, D., Wehnert, K. K., Hartmann, J., Schiffler, A., & Schmitt, J. (2021). Sustainable Aspects of a Metal Printing Process Chain with Laser Powder Bed Fusion (LPBF). *Procedia CIRP*, *98*, 613. https://doi.org/10.1016/j.procir.2021.01.163

[47] Cozzolino, E., Papa, I., & Astarita, A. (2025). Energy Assessment of Powder Bed Fusion Additive Manufacturing Processes at Industrial Scale: Experiments and Simulations. *Journal of Materials Engineering and Performance*. https://doi.org/10.1007/s11665-025-11007-w

[48] Rezaie, B., Anderson, A., Gallegos, S., & Azarmi, F. (2021). Present and Future Sustainability Development of 3D Metal Printing. *European Journal of Sustainable Development Research*, *5*(3). https://doi.org/10.21601/ejosdr/11132

[49] Ingarao, G., & Priarone, P. C. (2020). A comparative assessment of energy demand and life cycle costs for additive- and subtractive-based manufacturing approaches. *Journal of Manufacturing Processes*, *56*, 1219. https://doi.org/10.1016/j.jmapro.2020.06.009

[50] Cacace, S., Furlan, V., Sorci, R., Semeraro, Q., & Boccadoro, M. (2020). Using recycled material to produce gas-atomized metal powders for additive manufacturing processes. *Journal of Cleaner Production*, *268*, 122218. https://doi.org/10.1016/j.jclepro.2020.122218

[51] Nyamekye, P., Lakshmanan, R., Tepponen, V., & Westman, S. (2023). Sustainability aspects of additive manufacturing: Leverageing resource efficiency via product design optimisation and laser powder bed fusion. *Heliyon*, *10*(1). https://doi.org/10.1016/j.heliyon.2023.e23152

[52] Rahmani, R., Bashiri, B., Lopes, S. I., Hussain, A., Maurya, H. S., & Vilu, R. (2025). Sustainable Additive Manufacturing: An Overview on Life Cycle Impacts and Cost Efficiency of Laser Powder Bed Fusion. *Journal of Manufacturing and Materials Processing*, *9*(1), 18. https://doi.org/10.3390/jmmp9010018

[53] Jing, L., Tan, B., Jiang, S., & Ma, J. (2021). Additive manufacturing industrial adaptability analysis using fuzzy Bayesian Network. *Computers & Industrial Engineering*, *155*, 107216. https://doi.org/10.1016/j.cie.2021.107216

[54] Maresch, D., & Gartner, J. (2018). Make disruptive technological change happen - The case of additive manufacturing. *Technological Forecasting and Social Change*, *155*, 119216. https://doi.org/10.1016/j.techfore.2018.02.009

[55] Sandeep, B., Kannan, T. T. M., Chandradass, J., Ganesan, M., & Rajan, A. J. (2021). Scope of 3D printing in manufacturing industries-A review. *Materials Today Proceedings*, *45*, 6941. https://doi.org/10.1016/j.matpr.2021.01.394

[56] Jayakrishna, M., Vijay, M., & Khan, B. (2023). An Overview of Extensive Analysis of 3D Printing Applications in the Manufacturing Sector. *Journal of Engineering*, *2023*, 1. https://doi.org/10.1155/2023/7465737

[57] Pulatsu, E., & Lin, M. (2020). A review on customizing edible food materials into 3D printable inks: Approaches and strategies [Review of *A review on customizing edible food materials into 3D printable inks: Approaches and strategies*]. *Trends in Food Science & Technology*, *107*, 68. Elsevier BV. https://doi.org/10.1016/j.tifs.2020.11.023

[58] Lee, C. K. W., Xu, Y., Yuan, Q., Chan, Y. H. T., Poon, W. Y., Zhong, H., Chen, S., & Li, G. (2025). Advanced 3D Food Printing with Simultaneous Cooking and Generative AI Design. *Advanced Materials*. https://doi.org/10.1002/adma.202408282

[59] Bergonzi, L., Vettori, M., & Pirondi, A. (2019). Development of a miniaturized specimen to perform uniaxial tensile tests on high performance materials. *Procedia Structural Integrity*, *24*, 213. https://doi.org/10.1016/j.prostr.2020.02.018

[60] Strzelecki, P. (2019). Accuracy of determined S-N curve for constructional steel by selected models. *Fatigue & Fracture of Engineering Materials & Structures*, *43*(3), 550. https://doi.org/10.1111/ffe.13139

[61] Adhikari, A., & Chipara, M. (2024). A recent development trend in microwave radiation-based material engineering. *Polymer Bulletin*, *81*(10), 8527. https://doi.org/10.1007/s00289-023-05119-3

[62] Dillinger, B., Batchelor, A. R., Katrib, J., Dodds, C., Suchicital, C., Kingman, S., & Clark, D. (2020). Microwave digestion of gibbsite and bauxite in sodium hydroxide. *Hydrometallurgy*, *192*, 105257. https://doi.org/10.1016/j.hydromet.2020.105257

[63] Sun, J., Wang, W., & Yue, Q. (2016). Review on Microwave-Matter Interaction Fundamentals and Efficient Microwave-Associated Heating Strategies [Review of *Review on Microwave-Matter Interaction Fundamentals and Efficient Microwave-Associated Heating Strategies*]. *Materials*, *9*(4), 231. Multidisciplinary Digital Publishing Institute. https://doi.org/10.3390/ma9040231

[64] Zhou, X., Gezahegn, Y., Zhang, S., Tang, Z., Takhar, P. S., Pedrow, P., Sablani, S. S., & Tang, J. (2023). Theoretical reasons for rapid heating of vegetable oils by microwaves. *Current Research in Food Science*, *7*, 100641. https://doi.org/10.1016/j.crfs.2023.100641

[65] Horikoshi, S., Mura, H., & Serpone, N. (2023). Three-dimensional observations of the electric field distribution of variable frequency microwaves, and scaling-up organic syntheses. *Communications Chemistry*, *6*(1), 261. https://doi.org/10.1038/s42004-023-01062-6

[66] Seo, J., Han, G., & Hwang, H. (2025). Uniform temperature distribution in microwave heating achieved via rotating electric field. *Scientific Reports*, *15*(1), 17960. https://doi.org/10.1038/s41598-025-03373-1

[67] Chen, W., Malhotra, A., Yu, K., Zheng, W., Plaza-González, P. J., Catalá-Civera, J. M., Santamaría, J., & Vlachos, D. G. (2021). Intensified microwave-assisted heterogeneous catalytic reactors for sustainable chemical manufacturing. *Chemical Engineering Journal*, *420*, 130476. https://doi.org/10.1016/j.cej.2021.130476

[68] Liao, Y., Lan, J., Zhang, C., Hong, T., Yang, Y., Huang, K., & Zhu, H. (2016). A Phase-Shifting Method for Improving the Heating Uniformity of Microwave Processing Materials. *Materials*, *9*(5), 309. https://doi.org/10.3390/ma9050309

[69] Malhotra, A., Chen, W., Goyal, H., Plaza-González, P. J., Julián, I., Catalá-Civera, J. M., & Vlachos, D. G. (2021). Temperature Homogeneity under Selective and Localised Microwave Heating in Structured Flow Reactors. *Industrial & Engineering Chemistry Research*, *60*(18), 6835. https://doi.org/10.1021/acs.iecr.0c05580

[70] Ohmi, H., Kimoto, K., Nomura, T., Kakiuchi, H., & Yasutake, K. (2021). Study on silicon removal property and surface smoothing phenomenon by moderate-pressure microwave hydrogen plasma. *Materials Science in Semiconductor Processing*, *129*, 105780. https://doi.org/10.1016/j.mssp.2021.105780

[71] Zhu, H., Huang, K., & Tao, J. (2020). Special Issue on "Microwave Applications in Chemical Engineering." *Processes*, *8*(4), 491. https://doi.org/10.3390/pr8040491

[72] Singh, P., Goyal, D. K., & Bansal, A. (2021). Microwave heating: Fundasmentals and application in surface modification of metallic materials – A review [Review of *Microwave heating: Fundasmentals and application in surface modification of metallic materials – A review*]. *Materials Today Proceedings*, *43*, 564. Elsevier BV. https://doi.org/10.1016/j.matpr.2020.12.049

[73] Guan, C., Zhan, L., Zhang, D., Yao, S., Zhong, S., & Wang, B. (2023). Microwave uniformity regulation and its influence on temperature field distribution of composite materials. *Journal of Central South University*, *30*(10), 3374. https://doi.org/10.1007/s11771-023-5458-6

[74] Joardder, M. U. H., & Karim, A. (2025). Toward Uniform Microwave Heating in Food Drying: Principles, Technologies, and Emerging Trends. *Food Engineering Reviews*, *17*(4), 946. https://doi.org/10.1007/s12393-025-09426-5

[75] Yang, B., Han, Z., Cheng, C., Gao, H., & Wu, Z. (2023). Temperature uniformity optimisation with power-frequency coordinated variation in multi-source microwave based on sequential quadratic programming. *High Temperature Materials and Processes*, *42*(1). https://doi.org/10.1515/htmp-2022-0279

[76] Aver'yanova, I. O., Bogomolov, D. Yu., & Poroshin, V. V. (2017). ISO 25178 standard for three-dimensional parametric assessment of surface texture. *Russian Engineering Research*, *37*(6), 513. https://doi.org/10.3103/s1068798x17060053

[77] Marinello, F., & Pezzuolo, A. (2019). Application of ISO 25178 standard for multiscale 3D parametric assessment of surface topographies. *IOP Conference Series Earth and Environmental Science*, *275*(1), 12011. https://doi.org/10.1088/1755-1315/275/1/012011

[78] Yang, D., Tang, J., Xia, F., & Zhou, W. (2022). Rough Surface Characterisation Parameter Set and Redundant Parameter Set for Surface Modeling and Performance Research. *Materials*, *15*(17), 5971. https://doi.org/10.3390/ma15175971

[79] Lanzutti, A., Pujatti, M., Magnan, M., Andreatta, F., Nurmi, H., Silvonen, A., Hlede, E., & Fedrizzi, L. (2017). Uniaxial fatigue properties of closed die hot forged 42CrMo4 steel: Effect of flash and mechanical surface treatments. Materials & Design, 132, 400–408. https://doi.org/10.1016/j.matdes.2017.07.017

[80] Lanzutti, A., Sordetti, F., Magnan, M., Picco, N., Michelon, F., Sciarretta, F., Roncari, S., Zanetti, C., Pennè, W., Marin, E., & Fedrizzi, L. (2024). Effect of Surface Finish on Fatigue Properties of Ti Gr23 Alloy Produced by L PBF and to Be Used for Human Implants. In R. Montanari, M. Richetta, M. Febbi, & E. M. Staderini (Eds.), Engineering Methodologies for Medicine and Sports (EMMS 2024) (Mechanisms and Machine Science, Vol. 162, pp. 418–433). Springer, Cham. https://doi.org/10.1007/978-3-031-63755-1_31

[81] Arola, D., & Williams, C. L. (2002). Estimating the fatigue stress concentration factor of machined surfaces. International Journal of Fatigue, 24(9), 923–930. https://doi.org/10.1016/S0142-1123(02)00012-9

[82] Awd, M., Johannsen, J., Siddique, S., Emmelmann, C., & Walther, F. (2018). Qualification of selective laser-melted Al alloys against fatigue damage by means of measurement and modelling techniques. *MATEC Web of Conferences*, *165*, 2001. https://doi.org/10.1051/matecconf/201816502001

[83] Ngnekou, J. N. D., Nadot, Y., Hénaff, G., Nicolaï, J., & Ridosz, L. (2021). Effect of As-Built and Ground Surfaces on the Fatigue Properties of AlSi10Mg Alloy Produced by Additive Manufacturing. *Metals*, *11*(9), 1432. https://doi.org/10.3390/met11091432

[84] Al-Oraiqat, A. M., Смірнова, T., Drieiev, O., Смірнов, O., Polishchuk, L., Khan, S., Hasan, Y. M. Y., Amro, A. M., & Al-Rawashdeh, H. S. (2022). Method for Determining Treated Metal Surface Quality Using Computer Vision Technology [Review of *Method for Determining Treated Metal Surface Quality Using Computer Vision Technology*]. *Sensors*, *22*(16), 6223. Multidisciplinary Digital Publishing Institute. https://doi.org/10.3390/s22166223

[85] Berus, L., Skakun, P., Rajnović, D., Janjatović, P., Šidjanin, L., & Ficko, M. (2020). Determination of the Grain Size in Single-Phase Materials by Edge Detection and Concatenation. *Metals*, *10*(10), 1381. https://doi.org/10.3390/met10101381

[86] Sausto, F., Tezzele, C., & Beretta, S. (2022). Analysis of Fatigue Strength of L-PBF AlSi10Mg with Different Surface Post-Processes: Effect of Residual Stresses. *Metals*, *12*(6), 898. https://doi.org/10.3390/met12060898

[87] Tenkamp, J., Koch, A., Knorre, S., Krupp, U., Michels, W., & Walther, F. (2018). Influence of the microstructure on the cyclic stress-strain behaviour and fatigue life in hypo-eutectic Al-Si-Mg cast alloys. *MATEC Web of Conferences*, *165*, 15004. https://doi.org/10.1051/matecconf/201816515004

[88] Godec, Y. L., & Floch, S. L. (2023). Recent Developments of High-Pressure Spark Plasma Sintering: An Overview of Current Applications, Challenges and Future Directions [Review of *Recent Developments of High-Pressure Spark Plasma Sintering: An Overview of Current Applications, Challenges and Future Directions*]. *Materials*, *16*(3), 997. Multidisciplinary Digital Publishing Institute. https://doi.org/10.3390/ma16030997

[89] Manière, C., Lee, G., & Olevsky, E. A. (2017a). Proportional integral derivative, modeling and ways of stabilization for the spark plasma sintering process. *Results in Physics*, *7*, 1494. https://doi.org/10.1016/j.rinp.2017.04.020

[90] Manière, C., Lee, G., & Olevsky, E. A. (2017b). All-Materials-Inclusive Flash Spark Plasma Sintering. *Scientific Reports*, *7*(1). https://doi.org/10.1038/s41598-017-15365-x

[91] Prakasam, M., Balima, F., Cygan, S., Klimczyk, P., Jaworska, L., & Largeteau, A. (2019). Ultrahigh pressure SPS (HP-SPS) as new syntheses and exploration tool in materials science. In *Elsevier eBooks* (p. 201). Elsevier BV. https://doi.org/10.1016/b978-0-12-817744-0.00009-x

[92] Guillon, O., González-Julián, J., Dargatz, B., Kessel, T., Schierning, G., Räthel, J., & Herrmann, M. (2014). Field-Assisted Sintering Technology/Spark Plasma Sintering: Mechanisms, Materials, and Technology Developments. *Advanced Engineering Materials*, *16*(7), 830. https://doi.org/10.1002/adem.201300409

[93] Monchoux, J., Couret, A., Durand, L., Voisin, T., Trzaska, Z., & Thomas, M. (2021). Elaboration of Metallic Materials by SPS: Processing, Microstructures, Properties, and Shaping. *Metals*, *11*(2), 322. https://doi.org/10.3390/met11020322

[94] Kopeček, J., Bartha‖, K., Mušálek, R., Pala, Z., Chráska, T., Beran, P., Ryukhtin, V., Strunz, P., Nováková, J., Stráský, J., Novák, P., Heczko, O., Landa, M., Seiner, H., & Janeček, M. (2018). Structural characterisation of semi-heusler/light metal composites prepared by spark plasma sintering. *Scientific Reports*, *8*(1). https://doi.org/10.1038/s41598-018-29479-3

[95] Marchhart, T., Hargrove, C., Marin, A., Schamis, H., Saefan, A., Lang, E., Wang, X., & Allain, J. P. (2024). Discovering tungsten-based composites as plasma facing materials for future high-duty cycle nuclear fusion reactors. *Scientific Reports*, *14*(1). https://doi.org/10.1038/s41598-024-64614-3

[96] Laszkiewicz-Łukasik, J., Putyra, P., Klimczyk, P., Podsiadło, M., & Bednarczyk, K. (2021). Spark Plasma Sintering/Field Assisted Sintering Technique as a Universal Method for the Synthesis, Densification and Bonding Processes for Metal, Ceramic and Composite Materials. *Journal of Applied Materials Engineering*, *60*(2), 53. https://doi.org/10.35995/jame60020005

[97] Hitchcock, D., Livingston, R., & Liebenberg, D. H. (2015). Improved understanding of the spark plasma sintering process. *Journal of Applied Physics*, *117*(17). https://doi.org/10.1063/1.4919814

[98] Cavaliere, P. (2019). Spark Plasma Sintering of Materials. In *Springer eBooks*. Springer Nature. https://doi.org/10.1007/978-3-030-05327-7

[99] Chang, A., Zhang, B., Wu, Y., Zhao, Q., Zhang, H., Yao, J., Xu, J., & Zhao, P. (2015). Spark Plasma Sintering of Negative Temperature Coefficient Thermistor Ceramics. In *InTech eBooks*. https://doi.org/10.5772/59030

[100] Babalola, B. J., Ayodele, O. O., & Olubambi, P. A. (2023). Sintering of nanocrystalline materials: Sintering parameters [Review of *Sintering of nanocrystalline materials: Sintering parameters*]. *Heliyon*, *9*(3). Elsevier BV. https://doi.org/10.1016/j.heliyon.2023.e14070

[101] Ardigo-Besnard, M. R., Besnard, A., Pinot, Y., Bussière, F., Chateau-Cornu, J.-P., Vandenabeele, C., Lucas, S., Watiez, N., Descamps-Mandine, A., Josse, C., & Proietti, A. (2023). Austenitic-to-austenitic-ferritic stainless steel transformation via PVD powder surface functionalization and spark plasma sintering. *Materialia*, *33*, 102002. https://doi.org/10.1016/j.mtla.2023.102002

[102] Brucculeri, R., Airoldi, L., Baldini, P., Vigani, B., Rossi, S., Morganti, S., Auricchio, F., & Anselmi-Tamburini, U. (2022). Spark Plasma Sintering of Complex Metal and Ceramic Structures Produced by Robocasting. *SSRN Electronic Journal*. https://doi.org/10.2139/ssrn.4124411

[103] Hryha, E. (2025). Powder for Metal Additive Manufacturing: Production, Reuse and Recycling. *Journal of the Japan Society of Powder and Powder Metallurgy*, *72*. https://doi.org/10.2497/jjspm.14b-t6-03

[104] Sun, X., Chen, M., Liu, T., Zhang, K., Wei, H., Zhu, Z., & Liao, W. (2023). Characterisation, preparation, and reuse of metallic powders for laser powder bed fusion: a review [Review of *Characterisation, preparation, and reuse of metallic powders for laser powder bed fusion: a review*]. *International Journal of Extreme Manufacturing*, *6*(1), 12003. IOP Publishing. https://doi.org/10.1088/2631-7990/acfbc3

[105] Lanzutti, A., & Marin, E. (2024). The Challenges and Advances in Recycling/Re-Using Powder for Metal 3D Printing: A Comprehensive Review [Review of *The Challenges and Advances in Recycling/Re-Using Powder for Metal 3D Printing: A Comprehensive Review*]. *Metals*, *14*(8), 886. Multidisciplinary Digital Publishing Institute. https://doi.org/10.3390/met14080886

[106] Arrizubieta, J. I., Arrien, O. U., Ostolaza, M., & Múgica, A. (2020). Study of the Environmental Implications of Using Metal Powder in Additive Manufacturing and Its Handling. *Metals*, *10*(2), 261. https://doi.org/10.3390/met10020261

[107] Ferreira, B., Campos, A. A. de, Casati, R., Gonçalves, A., Leite, M., & Ribeiro, I. (2023). Technological capabilities and sustainability aspects of metal additive manufacturing. *Progress in Additive Manufacturing*, *9*(6), 1737. https://doi.org/10.1007/s40964-023-00534-4

[108] Lutter-Günther, M., Gebbe, C., Kamps, T., Seidel, C., & Reinhart, G. (2018). Powder recycling in laser beam melting: strategies, consumption modeling and influence on resource efficiency. *Production Engineering*, *12*, 377. https://doi.org/10.1007/s11740-018-0790-7

[109] Chen, R., Xin, J., Yang, Q., Chen, Z., Wu, Q., Li, S., Mao, A., & Wen, H. (2024). New insights into the high-temperature oxidation behaviour of (TiZrHfTaNb)C high-entropy carbide. *International Journal of Refractory Metals and Hard Materials*, *128*, 107018. https://doi.org/10.1016/j.ijrmhm.2024.107018

[110] Vidyuk, T. M., Ukhina, A. V., Gavrilov, A. I., Shikalov, V. S., Анисимов, А. Г., Lomovsky, O. I., & Dudina, D. V. (2023). Synthesis of Tungsten Carbides in a Copper Matrix by Spark Plasma Sintering: Microstructure Formation Mechanisms and Properties of the Consolidated Materials. *Materials*, *16*(15), 5385. https://doi.org/10.3390/ma16155385

[111] Cramer, C. L., Preston, A. D., Ma, K., & Nandwana, P. (2020). In-situ metal binder-phase formation to make WC-FeNi Cermets with spark plasma sintering from WC, Fe, Ni, and carbon powders. *International Journal of Refractory Metals and Hard Materials*, *88*, 105204. https://doi.org/10.1016/j.ijrmhm.2020.105204

[112] Pal, R., & Basak, A. (2022). Linking Powder Properties, Printing Parameters, Post-Processing Methods, and Fatigue Properties in Additive Manufacturing of AlSi10Mg. *Alloys*, *1*(2), 149. https://doi.org/10.3390/alloys1020010

[113] Bagherifard, S., Beretta, N., Monti, S., Riccio, M., Bandini, M., & Guagliano, M. (2018). On the fatigue strength enhancement of additive manufactured AlSi10Mg parts by mechanical and thermal post-processing. *Materials & Design*, *145*, 28. https://doi.org/10.1016/j.matdes.2018.02.055

[114] Fischer, C., & Schweizer, C. (2020). Lifetime assessment of the process-dependent material properties of additive manufactured AlSi10Mg under low-cycle fatigue loading. *MATEC Web of Conferences*, *326*, 7003. https://doi.org/10.1051/matecconf/202032607003

[115] Pandey, A., Chandra, C., & Gaur, V. (2025). An improved fatigue life prediction via defect-informed intelligent learning method. *International Journal of Mechanical Sciences*, 110885. https://doi.org/10.1016/j.ijmecsci.2025.110885

Acknowledgments

Scrivere i ringraziamenti è forse una delle parti più complesse di una tesi, perché impone di fermarsi e guardare indietro, dando un nome e un volto a ciò che ha reso possibile questo percorso. In questo momento di sintesi e riflessione, le colonne sonore di Hans Zimmer e le note di Ludovico Einaudi hanno fatto da sottofondo alla stesura di questo elaborato, accompagnandomi lungo le sue ultime pagine così come avevano fatto nei momenti più intensi del lavoro.

Desidero innanzitutto esprimere la mia profonda gratitudine al Prof. Paolo Veronesi, per avermi guidato con pazienza e rigore scientifico, per il tempo condiviso in laboratorio e per avermi trasmesso la passione per l'ambiente accademico. La fiducia che ha riposto nelle mie capacità ha trasformato una sfida complessa in una preziosa opportunità di crescita, non solo professionale ma anche personale.

Un sincero ringraziamento va alla Prof.ssa Elena Colombini, il cui entusiasmo e la cui visione hanno stimolato il mio interesse per questi temi, spingendomi costantemente oltre i miei limiti e contribuendo in modo decisivo alla realizzazione di questo lavoro.

Ringrazio la Prof.ssa Magdalena Gualtieri, le cui intuizioni, osservazioni puntuali e suggerimenti hanno rappresentato un contributo fondamentale allo sviluppo di questo percorso di ricerca.

Un ringraziamento speciale va al Prof. Farid, che mi ha accolto a Luleå durante il periodo di ricerca, offrendomi un ambiente ospitale, stimolante e ricco di confronto. La possibilità di lavorare al suo fianco e di approfondire i temi di questo studio in un contesto internazionale è stata un'esperienza preziosa, che ha ampliato le mie prospettive e ha arricchito in modo significativo questo elaborato. Un sentito grazie va anche a Marina, la mia supervisor durante le attività a Luleå, per il supporto costante, la disponibilità e l'attenzione con cui ha seguito ogni fase del lavoro.

Un ringraziamento speciale va a Enza, il mio quid pluris, la mia àncora. Mi ha accompagnato lungo ogni fase di questo cammino e, soprattutto, mi ha dato l'ispirazione per iniziarlo. Grazie per aver condiviso ogni passo di questo lungo viaggio. La tua

pazienza, davvero infinita, è stata il mio faro nei momenti di sconforto e la spinta a non mollare mai. A te va il mio ringraziamento più grande.

Ringrazio i miei genitori, Luca e Daniela, il piccolo Lorenzo e Roberto, il mio punto di appoggio più solido. Il vostro supporto morale e il vostro amore incondizionato sono stati una costante, nonostante un mare e molti chilometri di distanza. Grazie per esserci sempre stati.

Un ringraziamento speciale va anche ai genitori di Enza, Vito e Donata, a Donatello e Nellina, alle zie Italia e Carmela, e alla cara nonnina Vincenza. La loro accoglienza e il loro affetto mi hanno fatto sentire parte di una seconda famiglia, sempre pronta a sostenermi con gentilezza, calore e una presenza discreta ma costante. A tutti loro va la mia più sincera gratitudine, per aver reso questo percorso più leggero e più ricco di serenità.

Un ringraziamento speciale va anche a mio zio Franco, a zia Maria Pia e ai miei cugini Federico e Stefano. Nonostante la distanza abbia spesso segnato i nostri percorsi, la loro presenza costante, il loro affetto e il loro modo discreto ma sincero di esserci sono sempre stati per me una forza. A loro va un pensiero riconoscente e un ringraziamento speciale.

Un pensiero riconoscente va al mio storico allenatore Andrea, che durante le nostre sessioni in pista mi ha insegnato il valore della perseveranza, della disciplina e della capacità di non arrendersi, anche quando il percorso si fa difficile. Insegnamenti che hanno inciso profondamente nel mio modo di affrontare le sfide e che continuano ad accompagnarmi nel mio percorso, anche oggi.

Ringrazio Francesca, Mattia e Roberto, compagni di allenamento, amici e compagni di avventura. Grazie per le lunghe conversazioni, per il sostegno morale e per aver creduto in me anche nei momenti in cui io stesso faticavo a farlo.

Un grande pensiero va ad Annalisa, Antonio, Carmen, Cecilia, Emilio, Graziano, Giovanni, Paola, Paolo e Riccardo, gli amici di sempre. La vostra presenza è stata fondamentale. Senza di voi, questo traguardo non avrebbe avuto lo stesso significato.

Desidero infine ringraziare il mio manager Roberto, per avermi offerto la possibilità di intraprendere questo percorso in parallelo all'attività lavorativa. Il suo supporto, i

consigli mirati e la costante disponibilità sono stati determinanti per il buon esito di questo cammino.

Un sentito grazie va anche ai colleghi e amici, per aver contribuito a creare un ambiente stimolante e collaborativo, per l'aiuto concreto che ha permesso di ottimizzare tempi e attività nel corso degli anni e, non da ultimo, per le birre condivise dopo il lavoro, che hanno reso più leggeri anche i periodi più intensi.